RAB27B requirement for stretch-induced exocytosis in bladder umbrella cells

Luciana I. Gallo,[*‡¶] Marianela G. Dalghi,[*‡] Dennis R. Clayton,[*] Wily G. Ruiz, [*] Puneet Khandelwal,[*] and Gerard Apodaca[*†]

Departments of Medicine[*] and Cell Biology,[†] University of Pittsburgh, Pittsburgh, PA

[¶]Current address: Instituto de Fisiología, Biología Molecular y Neurociencias, Facultad de Ciencias Exactas y Naturales, Universidad de Buenos Aires, Consejo Nacional de Investigaciones Científicas y Técnicas, Buenos Aires, Argentina.

[‡] The first two authors contributed equally to this work.

Running title: Rab27b requirement for umbrella cell exocytosis

Address all correspondence to: Gerard Apodaca, Ph.D., University of Pittsburgh, Department of Medicine Renal-Electrolyte Division, 980 Scaife Hall, 3550 Terrace Street, Pittsburgh, PA, 15261. T-412-383-8893, F-412-383-8955/8956, e-mail: gla6@pitt.edu

Abbreviations used: DFVs, discoidal/fusiform-shaped vesicles; GAP, GTPase activating protein; GEF, guanine nucleotide exchange factor

Abstract

Umbrella cells, which must maintain a tight barrier, modulate their apical surface area during bladder filling by exocytosis of an abundant, subapical pool of discoidal- and/or fusiform-shaped vesicles (DFVs). Despite the importance of this trafficking event for bladder function, the pathways the promote DFV exocytosis remain to be identified. We previously showed that DFV exocytosis depends in part on a RAB11A-RAB8A-MYO5B network, but RAB27B is also reported to be associated with DFVs, and knockout mice lacking RAB27B have fewer DFVs. However, the RAB27B requirements for DFV exocytosis, and the relationship between RAB27B and the other umbrella cell-expressed RABs remains unclear. Using a whole-bladder preparation, we observed that filling-induced exocytosis of human growth hormone-loaded DFVs was significantly inhibited when RAB27B expression was down regulated using shRNA. RAB27A was also expressed in rat urothelium; however, RAB27A-specific shRNAs did not inhibit exocytosis, and the combination of RAB27A and RAB27B shRNAs did not significantly affect DFV exocytosis more than treatment with RAB27B shRNA alone. RAB27B and RAB11A showed a small degree of overlap when quantified using SQUASSH segmentation software, and expression of dominant-active or dominant-negative mutants of RAB11A or RAB8A, or expression of a RAB11A-specific shRNA, had no significant effect on the size, number, or intensity of RAB27B-positive DFVs. Likewise, treatment with RAB27B-specific shRNA had no effect on RAB11A-positive DFV parameters. We conclude that RAB27B, but not RAB27A, regulates DFV exocytosis in bladder umbrella cells in a manner that may be parallel to the previously described RAB11A-RAB8A-MYO5B pathway.

Introduction

To maintain its barrier function, the layer of umbrella cells that line the inner surface of the bladder must accommodate large variations in bladder volume during the micturition cycle. Whereas bladder filling stimulates the apical exocytosis of Discoidal- and/or Fusiform-shaped Vesicles (DFVs) in these cells (32, 45, 51), voiding triggers endocytosis of added apical membrane (30). Despite their physiological importance, we have limited insights into how these mechanically triggered trafficking events are regulated at the molecular level. One likely mechanism is through the action of Rab GTPases, a family comprised of 44 subfamilies in humans that play crucial roles in promoting vesicle movements, fusion, and fission during exocytosis (24). Work to date implicates three Rab GTPases in umbrella cell exocytosis: RAB11A, RAB8A, and RAB27B (10, 28, 29, 48). While RAB11A and RAB8A are traditionally thought to regulate endocytic recycling pathways, DFVs are formed in the *trans*-Golgi network, they cannot be labeled with endocytic tracers, and they are not lysosome-related organelles (17, 23, 29, 30). RAB11A is localized to DFVs and DFV exocytosis is dependent on this GTPase (29). DFV exocytosis also requires RAB8A, and like a variety of other trafficking situations (including lumen formation and ciliogenesis) (8, 11), RAB11A may act upstream of RAB8A to promote DFV exocytosis (28). The well-known effector of RAB11A and RAB8A, MYO5B, is also implicated in DFV exocytosis (28).

The other RAB associated with DFVs is RAB27, which has A and B isoforms (10, 48). RAB27 is a so-called “secretory” RAB, a family that includes RAB3 (A-D isoforms), RAB26, and RAB37. Members of this family are required for regulated secretion of secretory vesicles/granules in a number of different cell types (13). Mouse umbrella cells express RAB27B, but not RAB27A (10, 48); but, it is unknown if this expression pattern is universal across species. Electron microscopic studies unequivocally demonstrate that RAB27B is localized to DFVs, and recent studies show that RAB27B knockout mice have fewer DFVs than

controls (10, 48). However, other than these observations, there is no evidence that RAB27B regulates DFV exocytosis in umbrella cells. An additional unknown is the relationship of RAB27B to the putative RAB11A-RAB8A pathway. Based upon a modest degree of colocalization between RAB27B with RAB11A or RAB8A, and the position of the vesicles, it was recently proposed that RAB11A-RAB8A act upstream of the RAB27B-dependent step(s) (48), perhaps as part of a RAB cascade. However, the data thus far are limited and RAB27B and the RAB11A-RAB8A pathway could act in parallel pathways.

Our current studies establish that rat urothelium expresses both RAB27A and RAB27B. While downregulating RAB27B expression inhibits DFV exocytosis, downregulation of RAB27A does not. Colocalization analysis confirms that there is some overlap between RAB27B-labeled DFVs and those that express RAB11A or RAB8A (~ 10-20%). However, upon expression of dominant-active or dominant-negative mutants of RAB11A or RAB8A, or expression of a RAB11A-specific shRNA, we do not observe a significant effect on the size, number, or intensity of RAB27B-positive DFVs. Likewise, a reduction of RAB27B expression has no effect on RAB11A-positive DFVs. We propose that RAB27B regulates exocytosis in a pathway that may be distinct from that regulated by RAB11A-RAB8A. The implication of these findings for bladder function and mechanically regulated trafficking events is discussed.

Materials and Methods

Reagents and Antibodies

Unless specified otherwise, all chemicals were obtained from Sigma-Aldrich (St Louis, MO). Primary antibodies used in this study included the following: rabbit anti-hGH1 (National Hormone and Peptide Program, NHPP, Torrance, CA) or mouse monoclonal anti-hGH1 (ab15317, Abcam, Cambridge, MA); mouse monoclonal anti-KRT20 (M7019, clone Ks20.8, Dako, Carpinteria, CA), goat polyclonal anti-laminB receptor (sc-6216, Santa Cruz Biotechnology, Dallas, TX), mouse monoclonal anti-RAB8 (610844, clone 4, BD Biosciences, San Jose, CA), rabbit polyclonal antibodies and mouse monoclonal 8H10 antibody to RAB11A have been described (31); mouse monoclonal anti-RAB27A (MABN446, clone 16H2.1, EMD Millipore, Billerica, MA), rabbit polyclonal anti-RAB27B (HPA019849; Sigma-Aldrich); mouse monoclonal anti-MYO5A (M4812, Sigma-Aldrich), rabbit polyclonal anti-pan UPK (AUM) (kindly provided by T.T. Sun, New York University, New York); mouse monoclonal anti-UPK3A is previously described (44), and rabbit polyclonal anti-V5 (PA1-993, ThermoFisher, Grand Island, NY). Secondary antibodies included: Alexa488-, Dylight549-, Cy5-, or HRP-labeled affinity-purified and minimal cross-reacting goat or donkey secondary antibodies were purchased from Jackson ImmunoResearch (West Grove, PA). Rhodamine phalloidin and TO-PRO-3 were obtained from Molecular Probes-ThermoFisher.

Animals

Urinary bladders were obtained from female Sprague–Dawley rats (250–300 g). Rats were euthanized by inhalation of 100% CO_2, followed by a thoracotomy. All animal studies were performed under the approval of the University of Pittsburgh Institutional Animal Care and Use Committee.

HEK cell culture and transfection

HEK-293T cells (ThermoFisher) were routinely cultured in Complete Medium, which was comprised of DMEM high-glucose medium (Gibco-ThermoFisher) supplemented with 10% v/v FBS (Hyclone-GE HealthCare, Logan, UT) and 1:100 dilution of the following supplements: non-essential amino acids, penicillin/streptomycin, and glutamine (all from Gibco-ThermoFisher). Cells, cultured on 10-cm diameter dishes were incubated at 37˚ C in a cell culture incubator (Heraeus, Thermo-Fisher) gassed with a mixture of 5% v/v CO_2 / 95% v/v air. Prior to transfection, cells that were 90-95% confluent were trypsinized, centrifuged at 100 x *g*, and then resuspended in 10-ml of complete medium. One-ml of this cell suspension was placed in the bottom of each well of a 6-well dish. Transfection was performed using Lipofectamine 2000 reagent (ThermoFisher). For each cell well, 1.0 µg of DNA was diluted into 125 µl of Opti-MEM (Gibco-ThermoFisher) and 2.5 µl of Lipofectamine 2000 reagent was diluted into 125 µl of Opti-MEM. The two solutions were mixed, incubated for 5 min at ambient temperature, and then added to the well. Cells were incubated for 24-72 h prior to experimentation.

Sample preparation and Western blot analysis

HEK cells were cultured in 6-well dishes, as described above, whereas excised bladders were cut open along the midline and the tissue pinned out loosely on a rubber mat housed in a square culture dish filled with Kreb's buffer (110 mM NaCl, 25 mM $NaHCO_3$, 5.8 mM KCl, 1.2 mM $MgSO_4$, 1.2 mM KH_2PO_4, 11 mM glucose, 2 mM $CaCl_2$, pH 7.4 when gassed with 5% v/v CO_2). Prior to lysis, the medium covering the HEK cells or the buffer covering the split-open bladders was aspirated (except in the case where secretion of hGH1 or hGH1-V5 was assessed), the cell/tissue was rinsed with Kreb's buffer. Following aspiration, the HEK cells were dissolved in Lysis Buffer (100 mM NaCl, 50 mM TEA pH 8.6, 5 mM EDTA, 0.2% w/v NaN_3, 0.5% w/v SDS, supplemented with freshly-added 0.5 mM phenyl-methylsulfonylfluoride and 1:100 dilution of a protease inhibitor cocktail; catalog number P8340, Sigma-Aldrich). The

urothelial cells were dissolved by adding 60 µl of Lysis Buffer to the mucosal surface and collecting the fluid with P1000 Pipetman outfitted with a blue-tip. This process was repeated and the two lysates were pooled. The HEK cell lysate or urothelial cell lysate was collected into a 1.5-ml Eppendorf tube, and then shaken for 20 s at ambient temperature in a FastPrep 24 device (MP Biomedicals, San Diego, CA). Following centrifugation at 14,000 x g in an Eppendorf 5415D microfuge (Hauppauge, NY) for 5 min at 4˚ C, the supernatant was recovered and the protein concentration determined using bicinchoninic acid assay reagents (Pierce; Rockford, IL).

Samples (typically containing 10-25 µg of protein) were mixed with an equal volume of 2X Laemmli sample buffer, and the proteins resolved by SDS-PAGE using Criterion TGX 4-15% polyacrylamide gradient gels (BioRad, Hercules, CA), bathed in electrophoresis buffer (25 mM Tris, 192 mM glycine, 0.1% w/v SDS, pH 8.3), and exposed to 200 V constant current in a Criterion Cell electrophoresis device (BioRad). Proteins in the acrylamide gels were transferred to Immobilon-P (EMD-Millipore) in 100 mM CAPS, pH 11.0 buffer at 375 mA constant current for 40 min in a Mighty Small Transphor apparatus (Amersham Biosciences, Piscataway, NJ). The membrane was blocked for 1 h at ambient temperature with 5% (w/v) BSA in TBS-Tween (50 mM Tris-HCl, pH 7.5, 150 mM NaCl, 0.05% v/v Tween-20). After incubation with primary antibody (diluted in TBS-Tween containing 1% w/v BSA) overnight at 4˚ C, blots were washed with TBS-Tween (3 x 20 min on a shaker), incubated with HRP-conjugated anti-rabbit or anti-mouse antibodies (diluted in TBS-Tween containing 1% w/v BSA) for 60 min at ambient temperature, washed with TBS-Tween (3 x 20 min on a shaker), and immunoreactive protein species were visualized using SuperSignal West Substrate (Pierce; Rockford, IL) and exposure of the blot to Carestream Kodak BioMax MR Film (Sigma-Aldrich). The film was scanned to a 300 dpi TIFF file using a Perfection V750PRO flat-bed scanner (with transparency module; Epson, Long Beach, CA) interfaced with VueScan software (www.Hamrick.com), running on a PowerMac computer (Apple, Cupertino, CA). Alternatively, visualization and image capture was

performed using a Chemidoc Touch Imaging System (BioRad). Quantification of digital files was performed using ImageLab version 5.2.1 (Bio-Rad), running on an iMac computer.

RT-PCR

The urothelium was recovered by gentle scraping as described (5), the cells were lysed, and RNA was purified using the RNAqueous Micro kit (Life Technologies). RNA was treated with DNAse I and cDNA generated using the RETROscript First Strand Synthesis kit (Life technologies). PCR was performed using Taq polymerase (Life Technologies). The primers used are described in Table 1. Sequencing was used to confirm the identity of the PCR reaction products.

Tissue fixation, detection of antigens using immunofluorescence, and image acquisition

Excised rat bladders were cut open along the midline, rinsed with Krebs buffer, and then incubated in Krebs Buffer gassed with 5% v/v CO_2 for 30 min to allow the tissue to achieve a "relaxed" state. The tissue was subsequently fixed with 4% w/v paraformaldehyde in 100 mM Na-cacodylate buffer, pH 7.4 for 30 min, and then cryoprotected in 30% w/v sucrose (dissolved in phosphate-buffered saline, PBS) for 2 h. Bladders were embedded in cryomolds (15 x 15 x 5 mm; Fisher Scientific) filled with Optimal Cutting Temperature (OCT) solution (Tissue-Tek, Sakura Finetek, Torrance, CA), and frozen on dry ice. The blocks were stored at -70˚ C in tightly sealed plastic bags. Cryosections were cut using a Leica Microsystems CM1950 cryostat (Buffalo Grove, IL; 4 µm sections), and collected on Superfrost Plus glass slides (ThermoFisher Scientific, Pittsburgh, PA).

In most cases, sections were washed in PBS at room temperature and then unreacted fixative quenched by incubating the tissue slices for 10 minutes at room temperature with Quench Buffer (75 mM NH_4Cl and 20 mM glycine, pH 8.0 dissolved in PBS, containing 0.1% v/v Triton X-100). However, in the case of samples that were incubated with anti-RAB8 antibody,

193 the incubation in quench buffer was limited to 7 min, and then the tissue was incubated in
194 quench buffer containing 0.05% w/v SDS for 3 min. The tissue was then quickly rinsed three
195 times with PBS, and then three times for 5 min in the same buffer. All tissues were then
196 incubated in Block Solution (PBS containing 0.6% v/v fish skin gelatin, 0.05% w/v saponin) for
197 60 min at ambient temperature. Following incubation, the Block solution was aspirated, and
198 replaced with primary antibodies diluted in Block Solution and incubated overnight at 4˚ C in a
199 humid chamber. The second day, the slides were washed 3 times quickly and 3-times 5 min
200 with Block Solution, and then incubated with minimal cross-reactivity, fluorophore-labeled
201 secondary antibodies, diluted in Block Solution, for 1 h at ambient temperature. In some cases,
202 nuclei were counterstained with TO-PRO-3 (1:1000; ThermoFisher Scientific) and overall tissue
203 architecture visualized using tetramethylrhodamine isothiocyanate (TRITC)–labeled phalloidin
204 (ThermoFisher Scientific; 1:200), which labels cortical actin filaments. The labeled tissues were
205 then rinsed 3 times quickly and 3 times 5 min with Block Solution, rinsed with PBS, and then
206 postfixed in 4% w/v paraformaldehyde dissolved in 100 mM Cacodylate buffer, pH 7.4 for 5-10
207 min at ambient temperature. The slides were rinsed with PBS, excess liquid aspirated, and a
208 drop of SlowFade Diamond Antifade (Molecular Probes - ThermoFisher) was placed on the
209 tissue. Borosilicate coverslips (#1.5, 0.17 mm thickness, 24 x 50 mm; ThermoFisher) were
210 placed above the drop of mounting medium, excess mounting medium was removed by
211 aspiration, the edges of the coverslip were sealed with clear nail polish, and the slides stored at
212 -20˚ C until image acquisition was performed.
213 Images were captured using a Leica HCX PL APO 63X, 1.3 NA glycerol objective and the
214 appropriate laser lines of a Leica TCS SP5 CW-STED confocal microscope (in normal confocal
215 mode). The photomultipliers were set at 900-1200, signal and offset were optimized using the
216 Q-LUT option, and 8-bit images collected using 8 line averages combined with 6 frame
217 averages. Cross-talk between channels was prevented by use of spectral detectors coupled
218 with sequential scanning. Furthermore, we confirmed using TetraSpeck fluorescent

microspheres (0.5 μm and 0.2 μm; Molecular Probes-ThermoFisher) that there was limited pixel shift in images captured in the visible light spectrum. Stacks of images (1024 x 1024, 8-bit) were collected using a Z-step of 0.13 μm. For general microscopy, images were imported into Volocity 4-D software (Perkin Elmers; Waltham, MA), and following image reconstruction, exported as TIFF files. The contrast of the latter was corrected in Photoshop CC2015 (Adobe; San Jose, CA), and the composite images prepared in Adobe Illustrator CC2015.

Segmentation of digital images and measures of colocalization using the Squassh protocol

Segmentation of digital image files was performed using an implementation of the Squassh ("Segmentation and quantification of subcellular shapes") protocol, an open-source Java plugin for ImageJ and Fiji (39). The protocol combines user-settable parameters coupled with image denoising, deconvolution, and segmentation in 2D or 3D to detect objects, regardless of size and shape, and report parameters including intensity of objects, object number, size of objects, length of objects, and degree of colocalization based on overlap of object volumes. We used Fiji (version 2.0.0, downloaded from https://fiji.sc), and its automated update feature to download MosaicSuite (version July 2016) for ImageJ and Fiji (http://mosaic.mpi-cbg.de/?q=downloads/imageJ), which contains the Squassh protocol. Confocal image stacks (each comprised of five images) were collected using identical gain and offset for each marker imaged and saved in Leica (.lif) format. The image files were subsequently converted to two-channel TIFF image files using the .lif Extractor ImageJ macro (which must be loaded in Fiji using the Plugins → Macro → Install command and then subsequently implemented by using the Plugins → Macro → Run command). If data for only single channels were needed, we used the Image → Color → Split Channels command, saving the resulting single-colored image as a TIFF file. If a masked region of the image was needed, then drawing tools were used to select

those regions that would be masked and the Edit → Clear outside command was used (a black background was maintained using the Edit → Options → Colors → Background → Black command prior to the Clear outside command). The resulting image was then saved as a TIFF file.

A series of trials was performed to determine the optimal settings for segmentation of DFVs. Parameters defined included: regularization, minimal intensity threshold, and background subtraction (using a rolling ball algorithm). This process was performed iteratively, changing one parameter at a time, until images were obtained in which visibly-identifiable DFVs were automatically selected above background fluorescence and segmented from closely apposed neighbors (See Figures 1A-F). This was assessed by comparing sample images prior to processing with those images in which the outlines of segmented objects are superimposed upon the original image, or in which the identified segmented objects are displayed (Fig. 1B-C and movie S1). We used images of RAB27B with EEA1 as negative controls and fluorescent microspheres as positive controls (Fig. 1G).

The following scheme was ultimately used to process all image files in this manuscript. The Squassh protocol was initiated (Plugins → Mosaic → Segmentation → Squassh). After choosing the location of the image files on the computer (Apple PowerMac; multiple files are batch processed automatically by the software), the following parameters were input. Under "Background subtraction" a rolling ball = 5 was selected. For "Segmentation parameters," the following options were chosen: Regularization (ch1/ch2) = 0.025; Minimal Intensity Threshold (ch1/ch2) = 0.20; PSF model standard deviation in XY = 1.44 pixels and in Z = 2.54 pixels (Calculated using the following inputs: Emission = 519, Excitation = 496, Numerical aperture = 1.3, Refractive index of glycerol = 1.45, Pinhole = 1, Lateral pixel = 60.1 nm, Axial pixel = 125.9 nm); "Exclude Z-edge and Subpixal segmentation" = unchecked; Local intensity estimation = automatic; Noise model = Poisson; Region filter = none selected. For "Colocalization (two

channel images)" no options were selected. For "Visualization and output," Intermediate steps, Save object characteristics, and Outlines overlay were checked and in response to "set condition names and number of images per condition" we changed channel names as appropriate and under condition we input the number of like image stacks in the batch. At the end of the analysis, the software generates a series of image files, as well as summaries of colocalization and object data parameters in the following data files: stitch_ImageColoc.csv and stitch_ImageData.csv. These data files were opened in Microsoft Excel (Redmond, WA) using the import .csv option, and summary statistics collated.

The coefficient for colocalization, C_{size}, describes the fraction of total volume occupied by objects in one channel that overlap at least 50% with objects in the second channel. It is calculated as follows:

$$C_{size}(X_{Y+}/X) = \frac{\sum_{0 \in X} S_0 O_0}{\sum_{o \in X} S_0} \qquad C_{size}(Y_{X+}/Y) = \frac{\sum_{0 \in Y} S_0 O_0}{\sum_{o \in Y} S_0}$$

Where X is the set of all objects detected in channel 1, and Y is the set of all objects detected in channel 2. The notation X_{Y+} means the objects in channel one that share at least a 50% overlap of volume with objects in channel two. S_0 is the size of object 0 in pixels, $\Sigma_{0 \in X} S_0 0_0$ is the total size of colocalizing regions, and $\Sigma_{0 \in X} S_0$ is the total number of pixels occupied by all objects in that channel. $C_{size}(X_{Y+}/X)$ and $C_{size}(Y_{X+}/Y)$ may be identical or not, as one channel may have a broader distribution than the other one in the sampled region of the tissue.

Preparation of adenoviruses, identification of shRNAs, and in situ transduction of umbrella cells.

Adenoviruses expressing hGH1, GFP, GFP-tagged DN-Rab11aS_{25}N, GFP-tagged DA-Rab11aS_{20}V, RFP-tagged DA-Rab8aQ_{67}L and GFP-tagged DN-Rab8aT_{22}N were described previously (28, 29). To prepare hGH1-V5, cDNA encoding the entire coding region of hGH1, including signal sequence, fused in frame with the V5 epitope (GKPIPNPLLGLDST) was

293 synthesized by Integrated DNA Technologies, Inc. (Iowa) as a double-stranded gBlock gene
294 fragment. Restriction sites for BamHI and EcoRI were added at the 5' and 3' ends of the
295 construct, respectively, which were used to subclone the cDNA into the pAd-Lox plasmid.
296 Adenoviruses were prepared by the Viral Core Facility at the University of Pittsburgh.

297 To generate shRNAs, the following scheme was used. The iRNAi software
298 (Nucleobytes.com) was used to search the Rat RAB27A cDNA (Pubmed accession number
299 NM_017317.2), Rat RAB27B cDNA (Pubmed accession number NM_053459.1), or Rat
300 RAB11A cDNA (Pubmed accession number NM_031152.2) for optimal targets (typically 21-bp
301 in length). When possible, we sought sequences that were also found to be targets in mouse
302 and humans in the Mission Library validated shRNA sequence library (www.SigmaAldrich.com).
303 Four shRNA sequences were selected for each cDNA (Table 1). The top and the bottom
304 strands were individually synthesized (IDT, Coralville, IA) and annealed by mixing the two
305 strands in equal amounts, heating to 94° C and cooling gradually to room temperature. The
306 annealed shRNA sequences where then ligated into the pAd-Loss vector (25). The ability of the
307 different shRNA sequences to silence the Rab of interest was determined by co-transfecting
308 HEK293-T cells with the pAD-Loss vectors and the corresponding cDNA: rat RAB27A, which
309 was obtained from OpenBiosystems and subcloned into pEGFP-C3; RAB27B cDNA, which was
310 amplified from cDNA prepared from rat urothelial lysate. RAB27B was then subcloned into
311 pcDNA3.1; RAB11A cDNA was obtained from OpenBiosystems. Seventy-two h later, cells were
312 lysed, the proteins were resolved by SDS-PAGE, and RAB27A/B or RAB11A were detected by
313 western blotting using the techniques described above. One of each shRNA was selected for
314 further analysis: RAB27A-shRNA-2, RAB27B-shRNA-a and RAB11A-shRNA-1. Adenoviruses
315 were prepared by the Viral Core Facility at the University of Pittsburgh.

316 *In situ* transduction was performed as described previously (29). Briefly, rats were sedated
317 with 2% isoflurane and a 22-g Jelco IV catheter (Smith Medicals, Southington, CT), trimmed to
318 two-cm length, was introduced into the bladder via the urethra. The bladder was rinsed with

PBS, and filled with 400 µl of 0.1% w/v dodecyl-β-D-maltoside dissolved in PBS. The urethra was clamped, and after 5 min unclamped to allow the detergent to void. The latter step was facilitated by applying slight pressure to the lower abdomen. The bladder was filled with 400 µl PBS containing adenoviruses expressing the constructs described above (2.0×10^8 infectious virus particles, typically in a volume of 2-10 µl for each virus). The amount of scrambled-shRNA-expressing virus particles used was equal to the amount of specific shRNA virus particles used. The bladder was then clamped. After 30 min, the clamp was removed and the virus solution was allowed to void. The bladder was rinsed with PBS, anesthesia was discontinued, and the rats were allowed to revive. The rats were euthanized 2-4 days post transduction.

Measurement of hGH1-V5 secretion in ex-vivo bladder preparation

Rat bladders were transduced *in situ* with adenoviruses expressing hGH1-V5 in combination with scrambled-shRNA or RAB-specific shRNA as described above. Thirty-six-hours post infection, the animals were sacrificed by inhalation of CO_2 and the bladder along with the urethra were excised. A five-ml syringe, filled with Kreb's buffer warmed to 37˚ C, was attached to the Luer port of a 22-g Jelco catheter, which was trimmed to 2 cm in length. The catheter was gently inserted into the urethra, and the bladder was washed by slowly injecting 400 µL of Kreb's buffer (gassed with 5% v/v CO_2 / 95% v/v O_2) through the catheter, allowing the buffer to flow out of the bladder from the space between the catheter and urethral orifice. The rate of flow was adjusted so that the bladder did not appear to fill during the washing protocol. The catheter was then secured in place by placing a ligature around the urethra using silk suture material (Softsilk 6-0 suture, Covidien-Medtronic, Minneapolis, MN). The bladder was then incubated, undisturbed, for 30 min, submerged in a Petri dish, filled with Kreb's buffer, placed on a heating plate to maintain temperature at 37˚ C.

Subsequently, a syringe was inserted in the clamp of a model PhD Ultra syringe pump (Harvard Apparatus, Holliston, MA) and the bladder was slowly filled with 500 µL of Kreb's

buffer at a rate of 15 µL/min. The bladder was then allowed to incubate for an additional 30 min at 37˚ C before a 22-g needle, attached to a 5-mL syringe, was inserted through the bladder wall into the bladder lumen and all of the contents aspirated and then transferred to an Eppendorf tube, which was placed on ice. The bladder was then filled with 250 µL of Kreb's buffer (at a rate of 50 µl/min), the bladder contents were aspirated with a needle, and then pooled with the original lumen contents. The bladder was subsequently cut open along the midline, pinned out on a rubber mat, rinsed with Kreb's buffer, which was then removed by aspiration. A urothelial lysate was prepared by adding 65 µL of Lysis Buffer to the mucosal surface of the bladder and collecting the lysate with a blue tip attached to a P1000 Gilson Pipetman. This process was repeated one time and the two lysates combined. The lysates were then shaken 20 s at ambient temperature in a FastPrep-24 device to shear DNA.

The hGH1-V5 that was secreted (i.e., present in the bladder contents) or remaining cell associated (i.e., present in urothelial cell lysate) was recovered by immunoprecipitation using the following protocol. The pooled bladder contents containing secreted hGH1-V5 were mixed with 30 µL of SDS-lysis buffer, 30 µL of 2.5% v/v TX-100, and 15 µL of anti-V5 agarose beads (Sigma-Aldrich). The cell-associated fraction of hGH1-V5 was measured by taking one-quarter of urothelial lysate (typically 30 µL) and mixing it with 500 µl Kreb's buffer, 30 µL of 2.5% v/v TX-100, and 15 µL of anti-V5 agarose beads. The reactions were incubated overnight at 4˚ C on a Labquake rotator (Barnstead/Thermolyne, Dubuque, IA), the anti-V5 beads were recovered by a centrifugation for 1-min at 14,000 x g in a microfuge, washed with Kreb's buffer, and then recovered again by centrifugation. The washed beads were resuspended in 15 µl of 2X Laemmili sample buffer, heated at 99˚ C for 5 min, and processed for Western blots as described above.

Following image capture using the Chemidoc Touch Imaging System, the fraction of hGH1 secreted was quantified as follows. The optical density (OD) of hGH1-V5 was determined by drawing rectangles using the ImageLab Software (Biorad) volume tool. Rectangles of the same

size, but in regions of the gel lacking signal, were drawn to correct for background intensity. The background corrected OD signal of the bands corresponding to the bladder tissue lysate were multiplied by 4 to correct for the amount of lysate used in the immunoprecipitation. The ODs of total tissue associated hGH1-V5 and secreted hGH1-V5 were summed up, constituting the total hGH1-V5 expressed in a given bladder. The amount of secreted hGH1-V5 was calculated as the percentage of hGH1-V5 secreted with respect to the total amount expressed using the following equation:

$$\%hGH1V5_{\text{secreted}} = \frac{(OD\ \text{hGH1V5}_{\text{secreted}} - OD\ \text{background}) \times 100}{(OD\ \text{hGH1V5}_{\text{lysate}} - OD\ \text{background}) \times 4 + (OD\ \text{hGH1V5}_{\text{secreted}} - OD\ \text{background})}$$

This served to normalize the amount of secretion to the level of hGH1-V5 expressed in the umbrella cell layer, and was important to mitigate experiment-to-experiment variations in hGH1-V5 expression and detection of this construct.

Statistical analysis

Data are reported as mean ± S.E.M. Statistically significant differences between means were determined using a two-tailed Student's t-test; $P<0.05$ was considered statistically significant. One-way ANOVA, with Bonferonni's correction, was used when making multiple comparisons.

Results

Both RAB27A and RAB27B are expressed in rat urothelium

In mouse, RAB27B is reported to be expressed in the umbrella cell layer where it is associated with DFVs, whereas RAB27A is reported to be absent (10, 48). However, in rat urothelium we observed expression of both RAB27 isoforms. This was initially established using reverse-transcriptase PCR (RT-PCR), which revealed that message for both RAB27A and RAB27B were present in rat urothelial cDNA (Fig. 2A). In addition, we probed Western blots of urothelial lysates with nominally isoform-selective antibodies against RAB27A or RAB27B, both of which recognized ~ 25KD proteins (Fig. 2A). We confirmed the specificity of these antibodies by probing western blots of lysates prepared from HEK cell expressing GFP-RAB27A or GFP-RAB27B. The RAB27A antibodies reacted with GFP-RAB27A, but not GFP-RAB27B, and the RAB27B-selective antibodies we used reacted with GFP-RAB27B, but much less so with GFP-RAB27A (Fig. 2A).

We next immunolocalized RAB27B in rat urothelium. The three layers of this stratified epithelium were identified by co-staining with rhodamine-labeled phalloidin, which labels the cortical actin cytoskeleton. These layers include a superficial layer populated by large umbrella cells (~ 40 μm diameter in these samples), 1-2 layers of smaller intermediate cells (~ 10-15 μm diameter), and a single layer of basal cells (~ 10 μm in diameter), which rest on the basement membrane (Fig. 2B). We note that the urothelium, and the umbrella cell layer in particular, is highly deformable and can change its shape depending on the degree of filling or stretch applied prior to fixation, thus the variation in tissue architecture we sometimes observe. Within individual umbrella cells, RAB27B was concentrated in the apical cytoplasm (Fig. 2B). Less RAB27B was expressed in the underlying intermediate and basal cell layers.

Just below the subapical membrane actin cytoskeleton is a so-called “trajectorial network” of cytokeratins (including KRT20), which encase DFVs and which may modulate their traffic

toward the apical pole of the cell (46). We previously observed that while RAB11A-positive vesicles were mostly encased within the cytokeratin network, a population of RAB8A-positive vesicles were found past this network, and thus closer to the apical surface (28). Like the distribution of the latter, we observed that a population of RAB27B-positive vesicles also extended past this network (Fig. 2C), consistent with a recent report performed in mouse tissues (48). Because these RAB27B vesicles are very close to the apical membrane, they may be primed to undergo rapid fusion in response to stretch. We emphasize, however, that the localization of RAB27B-positive vesicles varied across the urothelium and these vesicles were also found deeper in the cytoplasm, including in and below the cytokeratin network.

The major cargoes of DFVs include the uroplakins (UPKs), which assemble into 16-nm asymmetric unit membrane particles sometimes after exiting the endoplasmic reticulum (49). We observed some coincidence between the RAB27B and uroplakin signals when merged images were examined by eye (Fig. 2D). This is consistent with a report by Chen et al., who demonstrated that RAB27B is localized to uroplakin-rich DFVs by immunoelectron microscopy (10). To quantify the degree of overlap in fluorescent signals, we previously used pixel-based methods of colocalization, but these can lead to overestimates of the degree of overlap as tissue sections are prone to higher levels of background staining than that observed in tissue culture cells, and RABs have both membrane-bound and cytosolic pools. For these studies, we used an automated segmentation software to detect individual vesicles in 3D and then to subsequently measure their degree of colocalization (assessed by measuring the overlap of volumes, see Methods for Squassh segmentation analysis). Using these techniques, we observed that ~ 12% of the RAB27B-positive vesicular structures co-localized with UPK-positive ones (Table 2), which is visibly similar to the degree of colocalization recently reported by Wankel et al. (but not quantified) (48). This degree of colocalization is relatively modest, likely reflecting the stringent conditions of colocalization we employed and reports that UPKs (assembled into plaques) are also found in endocytic structures (1, 20, 40).

We also measured the degree of overlap between RAB27B and its well-known bind partner MYO5A (14), an unconventional myosin motor that promotes RAB27B-dependent vesicle motility. We previously demonstrated that message for MYO5A (and MYO5B) is expressed in the urothelium (28), and in this study we observed that MYO5A was associated with vesicular elements distributed within the umbrella and underlying cell layers (Fig. 2E). Upon masking the non-umbrella cell-associated signal, we observed that RAB27B exhibited a modest degree of overlap with MYO5A (~ 16%; Table 2), which is consistent with recent observations (48).

Next, we assessed the distribution of RAB27A, and then quantified the degree of overlap between the RAB27A and RAB27B signals. Whereas the majority of RAB27B staining was concentrated in umbrella cells, and not in the underlying cell layers, the opposite was true for RAB27A: the RAB27A signal was concentrated in vesicular elements that populated the cytoplasm of intermediate and basal cells (marked with yellow and white circles, respectively Fig. 3A). Within umbrella cells, the distribution of RAB27A was similar to RAB27B. In either case, RAB27A/B was associated with small vesicular elements that accumulated under the apical surface. Upon masking out the non-umbrella cell signal, we estimated that ~ 37% of the umbrella cell RAB27B vesicle pool colocalized with RAB27A (Table 2).

RAB27B, but not RAB27A, regulates DFV exocytosis

As RAB27B was associated with at least a subset of DFVs, we next sought to determine if RAB27B regulated DFV exocytosis. We first identified a series of RAB27B-specific shRNAs, one of which was effective at down-regulating RAB27B expressed in HEK cells (RAB27B-ShRNA-a). This shRNA was expressed in the urothelium using adenoviral transduction (38), a method we have employed to express proteins and shRNAs in the urothelium (28-30, 34, 36). This technique has high transduction efficiency (75-95%), only the umbrella cell layer is targeted, and transduction does not perturb the barrier function or differentiation of the

urothelium. Using these methods, we observed that RAB27B-shRNA-a reduced endogenous RAB27B expression as assessed by immunofluorescence (Fig. 3B), or by western blots (Fig. 3C). In the latter case, expression was inhibited by ~90%.

To measure exocytosis, we took advantage of previous findings that when human growth hormone (hGH1) is expressed in the urothelium of transgenic mice, or in the urothelium of rats transduced with an adenovirus encoding hGH1, it is packaged into DFVs and released (exocytosed) into the bladder lumen in response to bladder filling (26, 29). No release is observed in the absence of stretch, indicating that there is little constitutive secretion of hGH1 in these cells (36). We confirmed that RAB27B colocalized with a subset of hGH1-labeled DFVs, particularly with those near the apical membrane (Fig. 3D and Table 2). To facilitate the ease by which exocytosed hGH1 is recovered from the extracellular fluid, we generated a construct in which a V5 epitope-tag was fused in frame to the C-terminus of hGH1 (hGH1-V5). This allowed for the recovery of hGH1-V5 released into extracellular fluid by way of immunoprecipitation (Fig. 3E). Finally, we used an *ex vivo* whole bladder preparation, which when transduced can be slowly filled with buffer and hGH1-V5 recovered from the urinary space (secreted) or from the cell-associated pool. Using these techniques, we observed that RAB27B-shRNA caused an ~ 45% reduction in the amount of hGH1-V5 released from the urothelium into the urinary space of transduced bladders (Fig. 4A).

We also identified a RAB27A-specific shRNA (RAB27A-shRNA-2), which significantly decreased RAB27A expression in HEK cells and in rat urothelium (Fig. 3C and data not shown). However, unlike the RAB27B-specific shRNA, the RAB27A-specific one had no significant effect on the release of hGH1-V5 in our exocytosis assay (Fig. 4B). We also tested the effect of simultaneously treating umbrella cells with both RAB27A- and RAB27B-specific shRNAs (Fig. 4C). While the combined shRNAs resulted in what appeared to be a greater degree of inhibition, this effect was not significantly different than treatment with RAB27B-shRNA alone. Taken

together, these results indicate that while a fraction of urothelial-associated RAB27A is expressed in the umbrella cell layer, only depletion of RAB27B significantly impairs exocytosis.

Neither RAB11A nor RAB8A regulate the size, number, or distribution of RAB27B-positive DFVs

Based in large part on the limited, visual overlap of their distributions in mouse tissue, it was proposed that RAB11A and RAB8A act upstream of RAB27B (48). We too observed a small degree of overlap between the signal for RAB27B and the signals for RAB11A or RAB8A in rat tissues (Fig. 5 and Table 2).

We posited that if RAB11A-RAB8A acts upstream of RAB27B, then expression of GDP-locked, dominant-negative mutants of RAB11A or RAB8A should affect the distribution, size, number, and/or intensity of RAB27B-positive vesicles. In contrast, expression of GTP-locked, dominant-active mutants may have the opposite effect. However, when compared to expression of GFP alone (control), expression of either dominant-negative-RAB8A or dominant-negative RAB11A had no obvious effect on the distribution of RAB27B in umbrella cells: RAB27B retained its vesicular appearance and the vesicles accumulated under the apical surface (Fig. 6A). Likewise, expression of dominant-active RAB8A or dominant-active RAB11A also had no obvious impact on the distribution of RAB27B. To further confirm these qualitative observations, we quantified the average size of RAB27B-labeled vesicles, the average fluorescent intensity of these vesicles, and the number of these vesicles in the confocal Z-stack. However, none of these parameters were significantly different from GFP-transduced controls, or from each other (Fig. 6B-D). Likewise, downregulating RAB11A expression using a RAB11A-specific shRNA, did not affect the size, average intensity, or number of RAB27B vesicles (Fig. 7A-B). We note that downregulating RAB11A-specific shRNA also caused a significant decrease in hGH secretion (Fig. 8). Unfortunately, we could not reliably detect whether the loss of both RAB11A and RAB27B caused an additive effect as the umbrella cell layer was morphologically impaired by

this treatment. We also asked whether RAB27B governs any qualitative or quantitative aspect of RAB11A-labeled vesicles. When compared to umbrella cells transduced with scrambled-shRNA, those transduced with RAB27B-shRNA exhibited no significant change in the distribution of RAB11A, or the size, intensity, or number of RAB11A-positive vesicles (Fig. 7C-D). Taken together, our results appear to argue against RAB8A or RAB11A acting upstream of RAB27B, or that RAB27B acts upstream of RAB11A.

Discussion

Exocytosis plays important roles in umbrella cell function and bladder physiology. During bladder filling, it allows the umbrella cell to increase its surface area, thus maintaining the urothelial barrier in the face of increasing fluid volume (27). Exocytosis also regulates the sensory and transducer functions of the urothelium by regulating the surface content of receptors and channels at the apical surface of the umbrella cells, the release of mediators such as ATP, and by governing tension in the apical membrane (27, 35, 47). While receptors and channels allow the urothelium to sense its extracellular milieu, the release of neurotransmitters including ATP allows the urothelium to communicate these changes to underlying afferent nerve processes, interstitial cells, and the detrusor (2). Regulation of tension determines how the urothelium will respond to wall tension as the bladder fills and empties (35). Thus, understanding how exocytosis in umbrella cells is modulated has broad implications for our understanding of bladder function. Including our current studies, we now know that RAB8A, RAB11A, RAB27A, and RAB27B are expressed in the urothelium and that all of these are associated in part with DFVs, an abundant population of vesicles that fills the apical cytoplasm of umbrella cells. Moreover, we previously demonstrated that RAB8A and RAB11A, acting in conjunction with MYO5B, regulate DFV exocytosis (28, 29).

Despite the undisputable evidence that RAB27B is associated with DFVs (10, 48), an open question is what is the function of RAB27B, if any, in DFV exocytosis. Qualitatively, the umbrella cells of RAB27B KO mice appear to have fewer DFVs than control mice (48). However, if DFV exocytosis depends on RAB27B, then one might expect that the umbrella cells from RAB27B KO mice would accumulate more DFVs in their cytoplasm, not fewer. It was hypothesized by Wankel et al. that crinophagy, an autophagy pathway that degrades excess secretory vesicles, accounts for this loss in vesicle number (48). However, in our studies we did not note a reproducible loss of hGH-labeled DFVs in rat bladders treated with RAB27B shRNA (as assessed by western blot). These dissimilar findings may reflect the different animal species employed in our two studies, or differences associated with the complete loss of RAB27B expression in KO mice versus downregulation of RAB27B expression by shRNA in rat bladders.

By using methods that allow us to label DFVs and measure exocytosis in whole bladders, we now show that umbrella cell exocytosis is dependent, at least in part, on RAB27B. We also observe that a pool of RAB27A is expressed in the umbrella cell layer (of the rat urothelium), where it has a similar distribution to RAB27B. This is different from mice, which apparently do not express RAB27A in the urothelium (10, 48). However, and unlike RAB27B, we find no significant effect of downregulating umbrella-cell RAB27A in our assays of exocytosis. While there is a trend toward increased inhibition when umbrella cells are transduced with both RAB27A-shRNA and RAB27B-shRNA, the effect is not significantly different than treatment with RAB27B-shRNA alone. The function of RAB27A in the urothelium remains to be described, although its expression in the intermediate and basal cells makes it likely that it is regulating exocytosis in these cell layers.

As we have now identified three RABs that regulate DFV exocytosis, what is the relationship of RAB27B to the RAB11A-RAB8A network? It was recently proposed that RAB11A and RAB8A are acting upstream of RAB27B (48). Indeed, such a relationship between these RABs has been described in MDCK cells undergoing *de novo* lumen formation during

cystogenesis (16). However, in our studies we cannot find a clear link between RAB27B and the RAB11A-RAB8A module. Expression of either dominant-active or dominant-negative mutants of RAB11A or RAB8A, or downregulating RAB11A expression in the umbrella cell layer, has no obvious impact on the distribution or size, intensity, or number of RAB27B-labeled DFVs. This lack of effect is unlikely to be the result of insufficient time of expression of these mutants, as we performed these assays after several days of transduction, sufficient time to significantly impair stretch-regulated exocytosis in umbrella cells. Moreover, RAB27B DFVs are unlikely to have a long half-life as they are exocytosed during each filling of the bladder, and upon voiding the majority of apical membrane is internalized and degraded in lysosomes (30, 45). We also observe that down-regulating RAB27B expression using shRNAs does not impact the distribution or size, intensity, or number of RAB11A-labeled DFVs. Taken together, these results argue against a simple relationship between RAB11A-RAB8A and RAB27B.

Instead, we hypothesize that umbrella cells may have at least two apically directed pathways: one regulated by RAB11A-RAB8A, and the other pathway regulated by RAB27B (Fig. 9). The site of biogenesis of these distinct populations of DFVs, is unknown but may occur as early as the trans-Golgi network (option 1, Fig. 9). In epithelial cells, there is ample precedence for having multiple apically directed pathways, a mechanism that has presumably evolved to allow the cell to differentially modulate the surface expression of functionally distinct classes of apical proteins (3, 4). The cargoes and associated regulatory molecules that are associated with these putative distinct populations of DFVs remain to be described, however, the presence of an asymmetric unit membrane (a feature of membranes containing UPKs assembled into 16-nm particles) in most if not all DFVs indicates that UPKs may be present as cargoes in all cases (19, 20). One possibility is that the exocytosis of mediators such as ATP may be differentially regulated than the exocytosis of membrane proteins such as UPKs or channels and receptors; however, nothing is known in this regard. Interestingly, we have described two differentially regulated pathways for exocytosis in umbrella cells (5, 37, 51): one

592 is called the “early stage,” and it requires the activity of stretch-sensitive ion channels and Ca^{2+};
593 the other is called the “late stage,” and is characterized by its requirements for ADAM17-
594 dependent HB-EGF cleavage, EGF receptor transactivation, MAPK activation, and protein
595 synthesis. Perhaps, each of these distinct exocytic pathways requires a different subset of
596 RABs.

597 If the umbrella cell has different populations of DFVs, then why is there any colocalization
598 of RAB27B with RAB11A or RAB8A? One possibility, is that all three GTPases are recruited
599 during an early step in the formation and/or maturation of DFVs, but then are subsequently
600 sorted from one another as distinct RAB11A-RAB8A DFVs and RAB27B DFVs are generated
601 (option 2, Fig. 9). However, it is also plausible that during DFV formation there is a significant
602 degree of cargo and possibly Rab mis-sorting. This may be true of other cell types as well, as a
603 large number of Rabs are associated with purified secretory granules (7, 9, 43).

604 In addition to cargoes (and RABs), it is expected that each population of DFVs will have a
605 trafficking machinery that is specialized for the vesicle population at hand. In this regard, we
606 know that the RAB11A-RAB8A cascade depends on MYO5B, which likely promotes transit
607 across the subapical actin barrier (28). RAB27B DFVs will also likely require a myosin motor to
608 pass the actin barrier, and the most likely candidate is MYO5A, which is a well-known effector of
609 RAB27B and which we and Wankel et al. recently showed is expressed in the urothelium and
610 shows some overlap with RAB27B (Fig. 9) (28, 48). It is worth noting that RAB8A, and possibly
611 RAB11A, can also bind to MYO5A (33, 42), which could explain the broader distribution of
612 MYO5A versus RAB27B in the umbrella cell layer. Interestingly, Wankel et al. also described a
613 number of SNAREs and RAB27B effector molecules that are expressed in the umbrella cell
614 layer (48). If these molecules are associated with all classes of DFVs or just a subset, and how
615 they modulate apical exocytosis will require additional experimentation.

616 Finally, understanding stretch-induced exocytosis in epithelial cells requires that we gain a
617 better understanding of not only the RABs involved, but also their associated GTPase-activating

proteins (GAPs) and guanine nucleotide exchange factors (GEFs), both of which are likely to be central to the mechanotransduction cascades that couple stretch to exocytosis. At present, there is limited, if any, information about the RAB-specific GAPs and GEFs that function in umbrella cells. GAPs have been described for RAB3A, RAB8A, RAB11A, and RAB27B (22, 41, 50), including the recently described RAB11A GAP TBC1D9B (15). Moreover, GEFs are known for RAB3A, RAB8A, and RAB27B (12, 18, 21), but no GEF for vertebrate RAB11A has been described. We do know that RAB3IP (*aliases* Rabin8/Rabin3), a GEF for RAB8A (18), is expressed in umbrella cells (28). Moreover, expression of wild-type RAB3IP or a dominant-negative variant of this protein that lacks GEF activity (Rabin8-L196A/F201A) stimulates, but does not inhibit stretch-induced exocytosis in umbrella cells (28). Interestingly, RAB3IP was originally described as a protein that interacts with RAB3A (6), However, it is unknown if RAB3 is expressed in the urothelium, and RAB3IP apparently does not act as a GEF for RAB3A (18). Future studies are needed to identify GAPs and GEFs in umbrella cells, with the ultimate goal of understanding how mechanical stimuli modulate membrane trafficking events such as DFV exocytosis, and how exocytosis in the urothelium governs bladder function.

Acknowledgements

The authors thank T.T. Sun (New York University) for his kind gift of anti-AUM antibodies. This work was supported NIH grants R01-DK104287 and P30-DK079307 (to G.A.), and by the Kidney Imaging Core of the Pittsburgh Center for Kidney Research (P30-DK079307).

References

1. **Amano O, Kataoka S, and Yamamoto T.** Turnover of asymmetric unit membranes in the transitional epithelial superficial cells of the rat urinary bladder. *Anatom Record* 229: 9-15, 1991.

2. **Apodaca G, Balestreire E, and Birder LA.** The uroepithelial-associated sensory web. *Kidney Intl* 72: 1057-1064, 2007.

3. **Apodaca G and Gallo LI.** Epithelial Polarity. In: *Colloquim series on building blocks of the cell: cell structure and function*, edited by Nabi IR: Morgan & Claypool Life Sciences, 2013.

4. **Apodaca G, Gallo LI, and Bryant DM.** Role of membrane traffic in the generation of epithelial cell asymmetry. *Nat Cell Biol* 14: 1235-1243, 2012.

5. **Balestreire EM and Apodaca G.** Apical EGF receptor signaling: regulation of stretch-dependent exocytosis in bladder umbrella cells. *Mol Biol Cell* 18: 1312-1323, 2007.

6. **Brondyk WH, McKiernan CJ, Fortner KA, Stabila P, Holz RW, and Macara IG.** Interaction cloning of Rabin3, a novel protein that associates with the Ras-like GTPase Rab3A. *Mol Cell Biol* 15: 1137-1143, 1995.

7. **Brunner Y, Coute Y, Iezzi M, Foti M, Fukuda M, Hochstrasser DF, Wollheim CB, and Sanchez JC.** Proteomics analysis of insulin secretory granules. *Mol Cell Proteomics* 6: 1007-1017, 2007.

8. **Bryant DM, Datta A, Rodriguez-Fraticelli AE, Peranen J, Martin-Belmonte F, and Mostov KE.** A molecular network for de novo generation of the apical surface and lumen. *Nature Cell Biol* 12: 1035-1045, 2010.

9. **Casey TM, Meade JL, and Hewitt EW.** Organelle proteomics: identification of the exocytic machinery associated with the natural killer cell secretory lysosome. *Mol Cell Proteomics* 6: 767-780, 2007.

10. **Chen Y, Guo X, Deng F-M, Liang F-X, Sun W, Ren M, Izumi T, Sabatini DD, Sun T-T, and Kreibich G.** Rab27b is associated with fusiform vesicles and may be involved in targeting uroplakins to urothelial apical membranes. *Proc Natl Acad Sci* 100: 14012-14017, 2003.

11. **Feng S, Knodler A, Ren J, Zhang J, Zhang X, Hong Y, Huang S, Peranen J, and Guo W.** A Rab8 guanine nucleotide exchange factor-effector interaction network regulates primary ciliogenesis. *J Bio Chem* 287: 15602-15609, 2012.

12. **Figueiredo AC, Wasmeier C, Tarafder AK, Ramalho JS, Baron RA, and Seabra MC.** Rab3GEP is the non-redundant guanine nucleotide exchange factor for Rab27a in melanocytes. *J Biol Chem* 283: 23209-23216, 2008.

13. **Fukuda M.** Regulation of secretory vesicle traffic by Rab small GTPases. *Cellular and molecular life sciences : CMLS* 65: 2801-2813, 2008.

14. **Fukuda M, Kuroda TS, and Mikoshiba K.** Slac2-a/melanophilin, the missing link between Rab27 and myosin Va. *J Biol Chem* 277: 12432-12436, 2002.

15. **Gallo LI, Liao Y, Ruiz WG, Clayton DR, Li M, Liu YJ, Jiang Y, Fukuda M, Apodaca G, and Yin XM.** TBC1D9B functions as a GTPase-activating protein for Rab11a in polarized MDCK cells. *Mol Biol Cell* 25: 3779-3797, 2014.

16. **Galvez-Santisteban M, Rodriguez-Fraticelli AE, Bryant DM, Vergarajauregui S, Yasuda T, Banon-Rodriguez I, Bernascone I, Datta A, Spivak N, Young K, Slim CL, Brakeman PR, Fukuda M, Mostov KE, and Martin-Belmonte F.** Synaptotagmin-like

684 proteins control the formation of a single apical membrane domain in epithelial cells.
685 *Nature cell biology* 14: 838-849, 2012.
686 17. **Guo X, Tu L, Gumper I, Plesken H, Novak EK, Chintala S, Swank RT, Pastores G,**
687 **Torres P, Izumi T, Sun T-T, Sabatini DD, and Kreibich G.** Involvement of Vps33a in the
688 fusion of uroplakin-degrading multivesicular bodies with lysosomes. *Traffic* (in press),
689 2009.
690 18. **Hattula K, Furuhjelm J, Arffman A, and Peranen J.** A Rab8-specific GDP/GTP
691 exchange factor is involved in actin remodeling and polarized membrane transport. *Mol*
692 *Biol Cell* 13: 3268-3280, 2002.
693 19. **Hicks M.** The mammalian urinary bladder: an accommodating organ. *Biol Rev* 50:
694 215-246, 1975.
695 20. **Hicks M, Ketterer B, and Warren R.** The ultrastructure and chemistry of the
696 luminal plasma membrane of the mammalian urinary bladder: a structure with low
697 permeability to water and ions. *Phil Trans Royal Soc London - Series B: Biol Sci* 268: 23-38,
698 1974.
699 21. **Horgan CP, Hanscom SR, and McCaffrey MW.** GRAB is a binding partner for the
700 Rab11a and Rab11b GTPases. *Biochem Biophys Res Commun* 441: 214-219, 2013.
701 22. **Hou Y, Chen X, Tolmachova T, Ernst SA, and Williams JA.** EPI64B acts as a
702 GTPase-activating protein for Rab27B in pancreatic acinar cells. *J Biol Chem* 288: 19548-
703 19557, 2013.
704 23. **Hudoklin S, Zupancic D, and Romih R.** Maturation of the Golgi apparatus in
705 urothelial cells. *Cell Tissue Res* 336: 453-463, 2009.

706 24. **Hutagalung AH and Novick PJ.** Role of Rab GTPases in membrane traffic and cell
707 physiology. *Physiol Rev* 91: 119-149, 2011.
708 25. **Kasahara H and Aoki H.** Gene silencing using adenoviral RNAi vector in vascular
709 smooth muscle cells and cardiomyocytes. *Methods Mol Med* 112: 155-172, 2005.
710 26. **Kerr DE, Liang F, Bondioli KR, Zhao H, Kreibich G, Wall RJ, and Sun TT.** The
711 bladder as a bioreactor: urothelium production and secretion of growth hormone into
712 urine. *Nat Biotechnol* 16: 75-79, 1998.
713 27. **Khandelwal P, Abraham SN, and Apodaca G.** Cell Biology and Physiology of the
714 Uroepithelium. *Am J Physiol Renal Physiol* 297: F1477-1501, 2009.
715 28. **Khandelwal P, Prakasam HS, Clayton DR, Ruiz WG, Gallo LI, van Roekel D,**
716 **Lukianov S, Peranen J, Goldenring JR, and Apodaca G.** A Rab11a-Rab8a-Myo5B network
717 promotes stretch-regulated exocytosis in bladder umbrella cells. *Mol Biol Cell* 24: 1007-
718 1019, 2013.
719 29. **Khandelwal P, Ruiz G, Balestreire-Hawryluk E, Weisz OA, Goldenring JA, and**
720 **Apodaca G.** Rab11a-dependent exocytosis of discoidal/fusiform vesicles in bladder
721 umbrella cells. *Proc Natl Acad Sci USA* 105: 15773-15778, 2008.
722 30. **Khandelwal P, Ruiz WG, and Apodaca G.** Compensatory endocytosis in bladder
723 umbrella cells occurs through an integrin-regulated and RhoA- and dynamin-dependent
724 pathway. *The EMBO journal* 29: 1961-1975, 2010.
725 31. **Lapierre LA, Dorn MC, Zimmerman CF, Navarre J, Burnette JO, and Goldenring**
726 **JR.** Rab11b resides in a vesicular compartment distinct from Rab11a in parietal cells and
727 other epithelial cells. *Exp Cell Res* 290: 322-331, 2003.

728 32. **Lewis S and de Moura J.** Incorporation of cytoplasmic vesicles into apical
729 membrane of mammalian urinary bladder epithelium. *Nature* 297: 685-688, 1982.
730 33. **Lindsay AJ, Jollivet F, Horgan CP, Khan AR, Raposo G, McCaffrey MW, and Goud**
731 **B.** Identification and characterization of multiple novel Rab-myosin Va interactions. *Mol*
732 *Biol Cell* 24: 3420-3434, 2013.
733 34. **Montalbetti N, Rued AC, Clayton DR, Ruiz WG, Bastacky SI, Prakasam HS, Eaton**
734 **AF, Kullmann FA, Apodaca G, and Carattino MD.** Increased urothelial paracellular
735 transport promotes cystitis. *Am J Physiol Renal Physiol*: ajprenal 00200 02015, 2015.
736 35. **Moulton DE, Sulzer V, Apodaca G, Byrne HM, and Waters SL.** Mathematical
737 modelling of stretch-induced membrane traffic in bladder umbrella cells. *J Theor Biol* 409:
738 115-132, 2016.
739 36. **Prakasam HS, Gallo LI, Li H, Ruiz WG, Hallows KR, and Apodaca G.** A1 adenosine
740 receptor-stimulated exocytosis in bladder umbrella cells requires phosphorylation of
741 ADAM17 Ser811 and EGF receptor transactivation. *Mol Biol Cell*, 2014.
742 37. **Prakasam HS, Herrington H, Roppolo JR, Jackson EK, and Apodaca G.**
743 Modulation of bladder function by luminal adenosine turnover and A1 receptor activation.
744 *Am J Physiol Renal Physiol* 303: F279-292, 2012.
745 38. **Ramesh N, Memarzadeh B, Ge Y, Frey D, VanRoey M, Rojas V, and Yu DC.**
746 Identification of pretreatment agents to enhance adenovirus infection of bladder
747 epithelium. *Mol Ther* 10: 697-705, 2004.
748 39. **Rizk A, Paul G, Incardona P, Bugarski M, Mansouri M, Niemann A, Ziegler U,**
749 **Berger P, and Sbalzarini IF.** Segmentation and quantification of subcellular structures in
750 fluorescence microscopy images using Squassh. *Nature protocols* 9: 586-596, 2014.

751 40. **Romih R and Jezernik K.** Endocytosis during postnatal differentiation in superficial
752 cells of the mouse urinary bladder epithelium. *Cell Biol Int* 18: 663-668, 1994.
753 41. **Sakane A, Manabe S, Ishizaki H, Tanaka-Okamoto M, Kiyokage E, Toida K,**
754 **Yoshida T, Miyoshi J, Kamiya H, Takai Y, and Sasaki T.** Rab3 GTPase-activating protein
755 regulates synaptic transmission and plasticity through the inactivation of Rab3. *Proc Natl*
756 *Acad Sci U S A* 103: 10029-10034, 2006.
757 42. **Sun Y, Chiu TT, Foley KP, Bilan PJ, and Klip A.** Myosin Va mediates Rab8A-
758 regulated GLUT4 vesicle exocytosis in insulin-stimulated muscle cells. *Mol Biol Cell* 25:
759 1159-1170, 2014.
760 43. **Takamori S, Holt M, Stenius K, Lemke EA, Gronborg M, Riedel D, Urlaub H,**
761 **Schenck S, Brugger B, Ringler P, Muller SA, Rammner B, Grater F, Hub JS, De Groot BL,**
762 **Mieskes G, Moriyama Y, Klingauf J, Grubmuller H, Heuser J, Wieland F, and Jahn R.**
763 Molecular anatomy of a trafficking organelle. *Cell* 127: 831-846, 2006.
764 44. **Truschel ST, Ruiz WG, Shulman T, Pilewski J, Sun T-T, Zeidel ML, and Apodaca**
765 **G.** Primary uroepithelial cultures: a model system to analyze umbrella cell barrier function.
766 *J Biol Chem* 274: 15020-15029, 1999.
767 45. **Truschel ST, Wang E, Ruiz WG, Leung SM, Rojas R, Lavelle J, Zeidel M, Stoffer D,**
768 **and Apodaca G.** Stretch-regulated exocytosis/endocytosis in bladder umbrella cells. *Mol*
769 *Biol Cell* 13: 830-846, 2002.
770 46. **Veranic P and Jezernik K.** Trajectorial organisation of cytokeratins within the
771 subapical region of umbrella cells. *Cell Motil Cytoskeleton* 53: 317-325, 2002.

47. **Wang ECY, Lee J-M, Ruiz WG, Balestreire EM, von Bodungen M, Barrick S, Cockayne DA, Birder L, and Apodaca G.** ATP and purinergic receptor-dependent membrane traffic in bladder umbrella cells. *J Clin Invest* 115: 2412-2422, 2005.

48. **Wankel B, Ouyang J, Guo X, Hadjiolova K, Miller J, Liao Y, Tham DK, Romih R, Andrade LR, Gumper I, Simon JP, Sachdeva R, Tolmachova T, Seabra MC, Fukuda M, Schaeren-Wiemers N, Hong WJ, Sabatini DD, Wu XR, Kong X, Kreibich G, Rindler MJ, and Sun TT.** Sequential and compartmentalized action of Rabs, SNAREs, and MAL in the apical delivery of fusiform vesicles in urothelial umbrella cells. *Mol Biol Cell* 27: 1621-1634, 2016.

49. **Wu XR, Kong XP, Pellicer A, Kreibich G, and Sun TT.** Uroplakins in urothelial biology, function, and disease. *Kidney Int* 75: 1153-1165, 2009.

50. **Yoshimura S, Egerer J, Fuchs E, Haas AK, and Barr FA.** Functional dissection of Rab GTPases involved in primary cilium formation. *J Cell Biol* 178: 363-369, 2007.

51. **Yu W, Khandelwal P, and Apodaca G.** Distinct apical and basolateral membrane requirements for stretch-induced membrane traffic at the apical surface of bladder umbrella cells. *Mol Biol Cell* 20: 282-295, 2009.

Name of primer or shRNA	Sequence	Predicted length of PCR product
ACTB PCR primers	FWD 5' CCCGCGAGTACAACCTTCTT 3' REV 5' AACACAGCCTGGATGGCTAC 3'	481 bp
RAB27A PCR primers	FWD 5' ACCAAACCGGGTAAAGCAGAG 3' REV 5' CATGCTCACTCGGTGTCTCA 3'	715 bp
RAB27B PCR primers	FWD 5' GACTGTGACTCTGTGAGGCTG 3' REV 5' CTGCAGTTGACTCATCCAGTT 3'	508 bp
RAB27A-shRNA-1	5' gctgccaatgggacaaacata 3'	
RAB27A-shRNA-2	**5' gcttctgttcgacctgacaaa 3'**	
RAB27A-shRNA-3	5' ttcatcaccacagtgggca 3'	
RAB27A-shRNA-4	5' ccagtacactgatgggaagtt 3'	
RAB27B-shRNA-a	**5' gcataccatactttgaaacaa 3'**	
RAB27B-shRNA-b	5' ccttctggacttaatcatgaa 3'	
RAB27B-shRNA-c	5' ccagtcaacagagtttctt 3'	
RAB27B-shRNA-d	5' gtcaactgcaggcaaatgct 3'	
RAB11A-shRNA-1	**5' gcctcctgtctcgatttact 3'**	
RAB11A-shRNA-2	5' tctggaaagcaagagtacc 3'	
RAB11A-shRNA-3	5' tggtttgtcgttcattgag 3'	
RAB11A-shRNA-4	5' tgtggttcctattcatgtc 3'	
Scrambled-shRNA	**5' gtcggatttcctggtatatgt 3'**	

790 **Table 1.** Primers (PCR) and target sequences for shRNAs used in analysis. The shRNAs used

791 in the urothelium are bolded.

792

Colocalization pair (X_{Y+} / X or Y_{X+} / Y)	C_{size}	N
$RAB27B_{UPK}$ / RAB27B	0.12 ± 0.00	3
UPK_{RAB27B} / UPK	0.05 ± 0.01	3
$RAB27B_{RAB27A}$ / RAB27B	0.40 ± 0.02	4
$RAB27A_{RAB27B}$ / RAB27A	0.45 ± 0.03	4
$RAB27B_{MYO5A}$ / RAB27B	0.16 ± 0.01	3
$MYO5A_{RAB27B}$ / MYO5A	0.12 ± 0.01	3
$RAB27B_{HGH1}$ / RAB27B	0.40 ± 0.06	4
$HGH1_{RAB27B}$ / HGH1	0.30 ± 0.02	4
$RAB27B_{RAB11A}$ / RAB27B	0.096 ± 0.02	4
$RAB11A_{RAB27B}$ / RAB11A	0.06 ± 0.00	4
$RAB27B_{RAB8A}$ / RAB27B	0.22 ± 0.05	4
$RAB8_{RAB27B}$ / Rab8A	0.23 ± 0.03	4
$RAB27B_{EEA1}$ / RAB27B	0.01 ± 0.00	4
$EEA1_{RAB27B}$ / EEA1	0.03 ± 0.00	4
Fluorescent spheres	1.0 ± 0.0	1
Fluorescent spheres	1.0 ± 0.0	1

793

794 **Table 2.** Degree of colocalization measured for the indicated pair of markers using Squaash
795 segmentation software. Data are mean ± SEM; N is equal to the number of rats, with ≥ 3
796 random images analyzed from each animal.
797
798

Figure Legends

Fig. 1. Segmentation of DFV immunofluorescense using Squassh software. (A) Example confocal image showing the distribution of RAB27B and RAB11A in the urothelium. **(B-C)** The image in panel A was processed using the following Squassh software parameters determined to be optimal to detect the vast majority of Rab-positive DFVs, well segmented from one another, in a large number of image files: regularization = 0.025, minimum intensity = 0.20, and background correction using a rolling ball = 5 px. In B, the segmented objects in the RAB27B (green) channel are outlined (see bottom panels for magnified view of boxed region in top panel). Note, that the outlined vesicles identified by the software are surrounded by low levels of non-vesicular fluorescence. Values for pixel-based measures of colocalization including Pearson's correlation coefficient and Mander's coefficients (both corrected using the automated Coste's threshold routine) are calculated for the image in panel A using the JACoP plugin for ImageJ. These values indicate a higher degree of colocalization than is apparent from optical inspection of the image and are likely affected by the aforementioned non-vesicular fluorescence. In C, the segmented RAB27B (green) and RAB11A (red) objects are depicted as a maximum projection and regions of colocalization (i.e, those that have a 50% or greater overlap of their volumes) are shown in yellow. **(D-F)** A series of trials showing the effects of changing the values for regularization, minimal intensity threshold, and background subtraction (i.e., rolling ball). The results of changing these parameters on C_{size} and the number of detected objects is found to the left and right of each panel, respectively. The parameter with the largest effect on segmentation was the value set for the rolling ball: too high, there was limited separation of DFVs from one another, and set too low, there was limited colocalization. The regularization or minimal intensity parameters affected the number of objects detected, with smaller values resulting in more objects detected. In addition, smaller values for these parameters increased the degree of colocalization, but at the expense of enlarging the objects

and dramatically increasing the computer time needed to perform the analysis. **(G)** We used images of RAB27B with EEA1 as negative controls, and 0.5 µm fluorescent microspheres as positive controls for our analysis. The long axis of DFVs is ~ 0.5 µm. Values for C_{size} were determined using the parameters described for panels B-C.

Fig. 2. Expression of RAB27A and RAB27B in rat urothelium. (**A**) left panels: RT-PCR was used to demonstrate expression of RAB27A and RAB27B in rat urothelial cDNA, and Western blots were used to confirm RAB27A/B protein expression in urothelial lysates. Right panels: GFP-RAB27A or GFP-RAB27B were expressed in HEK cells and the specificity of the RAB27A- and RAB27B-specific antibodies confirmed by Western blot. (**B**) Distribution of RAB27B, nuclei (labeled with lamin-B), and actin (labeled with TRITC-phalloidin) in rat urothelium. The position of the umbrella cells (UC), intermediate cells (white-colored circles), and basal cells (yellow-colored circles) are indicated. Images are projections of a confocal Z-series. (**C**) Distribution of RAB27B, actin, and KRT20 in rat urothelium. Images are projections of a confocal Z-series. (**D**) Distribution of RAB27B and UPK3A in rat urothelium. Images are projections of a confocal Z-series. The image to the right shows the Z-stack after processing with Squassh segmentation software. The segmented objects (RAB27B = green and UPK3A = red) are shown at maximum intensity, and yellow areas indicate regions of colocalization (≥ 50% overlap of volumes). (E) Distribution of MYO5A and RAB27B in rat urothelium. The results of Squassh segmentation is shown in the right-most panel.

Fig. 3. Localization of RAB27A, characterization of RAB27A and RAB27B shRNAs, and confirmation of hGH1-V5 secretion. **(A**) Distribution of RAB27B, nuclei (labeled with TO-PRO-3), and RAB27A in rat urothelium. The position of the umbrella cells (UC), intermediate cells (white-colored circles), and basal cells (yellow-colored circles) are indicated. Images are projections of a confocal Z-series. The image to the right shows the Z-stack after processing with Squassh

segmentation software. The segmented objects (RAB27B = green and RAB27A = red) are shown at maximum intensity, and yellow areas indicate regions of colocalization (≥ 50% overlap of volumes). (**B**) Rat bladders were transduced with Scrambled (Scr)-shRNA or RAB27B-shRNA-a and the distribution of RAB27B and actin were assessed in fixed urothelial tissues. The position of umbrella cells (UC) are indicated. Images are projections of a confocal Z-series. (**C**) Left panels: Rat bladders were transduced with the indicated shRNA and lysates probed with antibodies specific for RAB27A, RAB27B, or GAPDH (loading control). Right panels: Quantification of the amount of RAB27B (top) or RAB27A (bottom) expression in bladders transduced with RAB27B-shRNA-a, RAB27A-shRNA-2, or Scrambled (Scr)-shRNA. (**D**) Rat bladders were transduced with adenovirus encoding hGH1, and the distribution of hGH1, RAB27B, and actin assessed in fixed urothelium. Images are projections of a confocal Z-series. The image to the right shows the masked image after processing with Squassh segmentation software. The segmented objects (hGH1 = green and RAB27B = red) are shown at maximum intensity, and yellow areas indicate regions of colocalization (≥ 50% overlap of volumes). (**E**) HEK293 cells were transfected with hGH1 or hGH1-V5. The cells were incubated overnight at 37˚ C and the presence of hGH1 or the V5 epitope tag in the cell lysate or cell medium (secreted) was detected by Western blot. The hGH1-V5 was immunoprecipitated from the medium using anti-V5 antibodies, and detected using antibodies against hGH1. The asterisk shows background binding of hGH1 under the washing protocol used in our assay.

Fig. 4. Inhibition of hGH1-V5 release by transduction with adenovirus encoding RAB27B-shRNA-a. **(A-C)** Rat bladders were transduced with adenoviruses encoding hGH1-V5 and either scrambled (Scr)-shRNA, RAB27B-shRNA-a alone (A), RAB27A-shRNA-2 alone (B), or both RAB27B-shRNA-a and RAB27A-shRNA-2 (C). Bladders were excised, filled with buffer, and the amount of hGH1-V5 released in the bladder lumen (secreted) or remaining cell associated was immunoprecipitated and detected by Western blot analysis using an anti-hGH1 antibody. Each

experiment included samples from rat bladders transduced with scrambled-shRNA and either RAB27A-specific shRNAs and/or RAB27B-specific shRNA. The samples were processed side-by-side and Western blots developed simultaneously for each experiment. The total amount of secreted hGH1-V5 and its corresponding cell associated fraction (1/4th of the total) are shown for each condition.

Fig. 5. Distribution of RAB27B, RAB11A, and RAB8A in rat urothelium. **(A-B)** Localization of RAB27B and either RAB11A (A) or RAB8A (B). Images are projections of confocal Z-series. The image to the right shows the Z-stack after processing with Squassh segmentation software. The segmented objects (RAB27B = green and RAB11A/RAB8A = red) are shown at maximum intensity, and yellow areas indicate regions of colocalization (≥ 50% overlap of volumes).

Fig. 6. Effect of expressing mutants of RAB11A and RAB8A on the distribution, size, intensity, and number of RAB27B vesicles. Bladders were transduced with adenoviruses encoding GFP alone (control), or GFP-tagged dominant negative (DN) RAB8A, or RFP-tagged dominant active (DA) RAB8A, GFP-tagged DN-RAB11A, or GFP-tagged DA-RAB11A. (**A**) Confocal analysis. The left-most column shows expression of the indicated protein (green), the middle column shows the distribution of RAB27B in the tissue (red), and the right-most column shows the Z-stack after cell masking and Squassh segmentation analysis of the RAB27B channel. (**B-D**) Summary statistics for the size (B), intensity (C), and number of RAB27B vesicles in cells expressing the indicated protein. None of the values are significantly different from GFP controls or from one another (assessed using ANOVA).

Fig. 7. Effect of depleting RAB11A or RAB27B on the distribution, size, intensity, and number of DFVs. Bladders were transduced with adenoviruses encoding Scrambled-shRNA, RAB11A-shRNA-1 or RAB27B-shRNA-a. (**A**) Confocal images showing the distribution of RAB27B and

RAB11A in transduced urothelial tissue. The non-mucosal surfaces of the urothelium were labeled using an antibody to CLD4. (**B**) Summary statistics for the size, intensity, and number of RAB27B-positive vesicles in cells transduced with the indicated shRNA. None of the values are significantly different from Scrambled-shRNA controls (assessed using t-tests). **(C)** Confocal images showing the distribution of RAB27B and RAB11A in transduced urothelial tissues. The cortical actin cytoskeleton of the urothelium was labeled using rhodamine-phalloidin. (**D**) Summary statistics for the size, intensity, and number of RAB11A-positive vesicles in cells transduced with the indicated shRNA. None of the values are significantly different from Scrambled-shRNA controls (assessed using t-tests).

Fig. 8. Inhibition of hGH1-V5 release by transduction with adenovirus encoding RAB11A-shRNA-1. Rat bladders were transduced with adenoviruses encoding hGH1-V5 and either scrambled (Scr)-shRNA or RAB11A-shRNA-1. The amount of secreted hGH1-V5 is shown.

Fig. 9. Model for RAB-dependent DFV exocytosis in bladder umbrella cells. See text for explanation.

Movie S1. Validation of Squassh segmentation analysis. This video shows the localization of RAB27B (green) and RAB11A (red) before and after Squaash segmentation. Note that the segmented objects are shown at their maximum intensity, and yellow areas indicate regions of colocalization (≥ 50% overlap in object volumes). The movie is best viewed with the end user's video software set to "loop" mode.

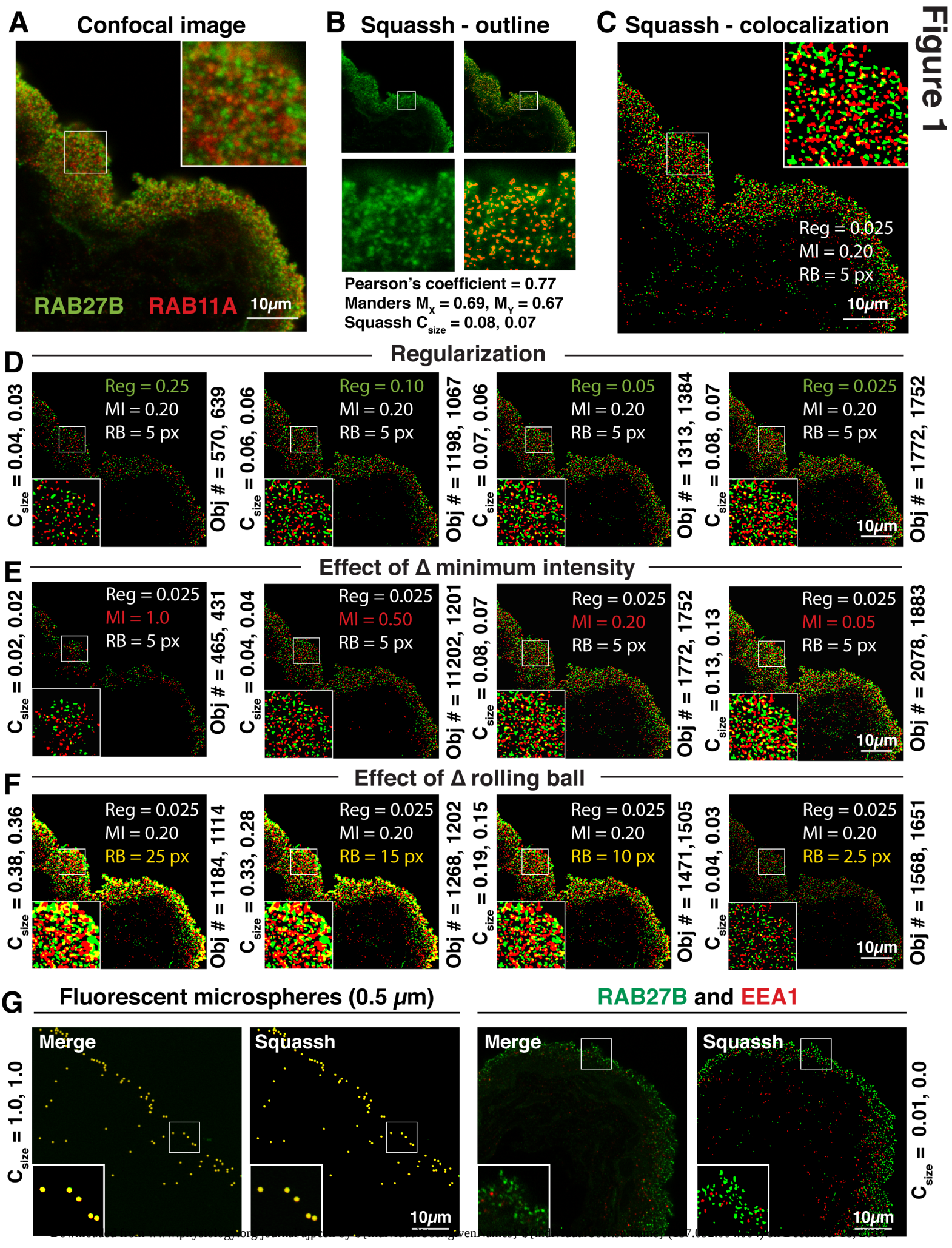
Figure 1
A Confocal image
RAB27B RAB11A 10μm
B Squassh - outline
Pearson's coefficient = 0.77
Manders M_X = 0.69, M_Y = 0.67
Squassh C_{size} = 0.08, 0.07
C Squassh - colocalization
Reg = 0.025
MI = 0.20
RB = 5 px
10μm
D Regularization
Reg = 0.25 MI = 0.20 RB = 5 px
C_{size} = 0.04, 0.03
Obj # = 570, 639
Reg = 0.10 MI = 0.20 RB = 5 px
C_{size} = 0.06, 0.06
Obj # = 1198, 1067
Reg = 0.05 MI = 0.20 RB = 5 px
C_{size} = 0.07, 0.06
Obj # = 1313, 1384
Reg = 0.025 MI = 0.20 RB = 5 px
C_{size} = 0.08, 0.07
Obj # = 1772, 1752
10μm
E Effect of Δ minimum intensity
Reg = 0.025 MI = 1.0 RB = 5 px
C_{size} = 0.02, 0.02
Obj # = 465, 431
Reg = 0.025 MI = 0.50 RB = 5 px
C_{size} = 0.04, 0.04
Obj # = 11202, 1201
Reg = 0.025 MI = 0.20 RB = 5 px
C_{size} = 0.08, 0.07
Obj # = 1772, 1752
Reg = 0.025 MI = 0.05 RB = 5 px
C_{size} = 0.13, 0.13
Obj # = 2078, 1883
10μm
F Effect of Δ rolling ball
Reg = 0.025 MI = 0.20 RB = 25 px
C_{size} = 0.38, 0.36
Obj # = 1184, 1114
Reg = 0.025 MI = 0.20 RB = 15 px
C_{size} = 0.33, 0.28
Obj # = 1268, 1202
Reg = 0.025 MI = 0.20 RB = 10 px
C_{size} = 0.19, 0.15
Obj # = 1471,1505
Reg = 0.025 MI = 0.20 RB = 2.5 px
C_{size} = 0.04, 0.03
Obj # = 1568, 1651
10μm
G Fluorescent microspheres (0.5 μm)
RAB27B and EEA1
Merge
Squassh
C_{size} = 1.0, 1.0
Merge
Squassh
C_{size} = 0.01, 0.0
10μm

Figure 2

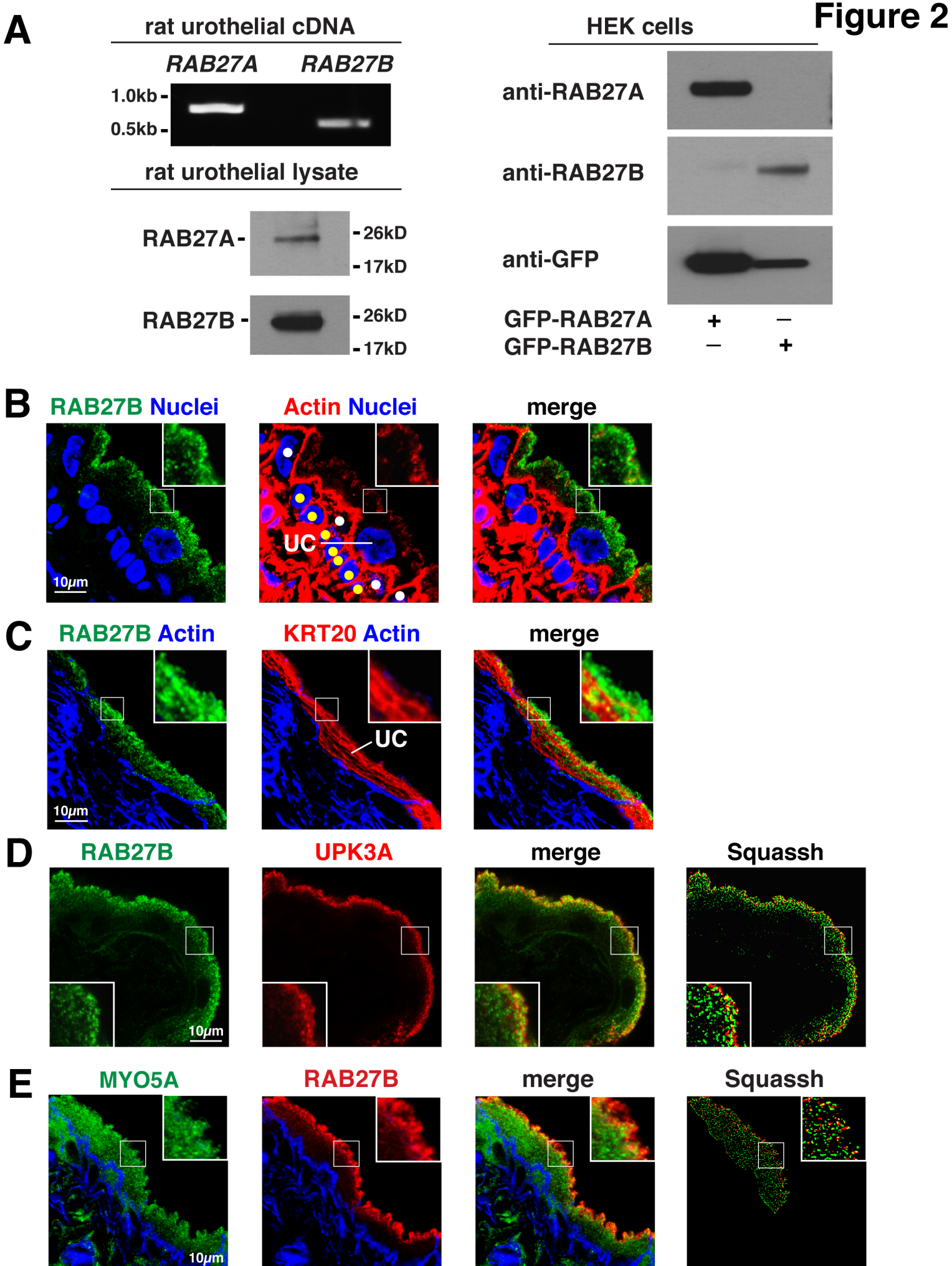

Figure 3

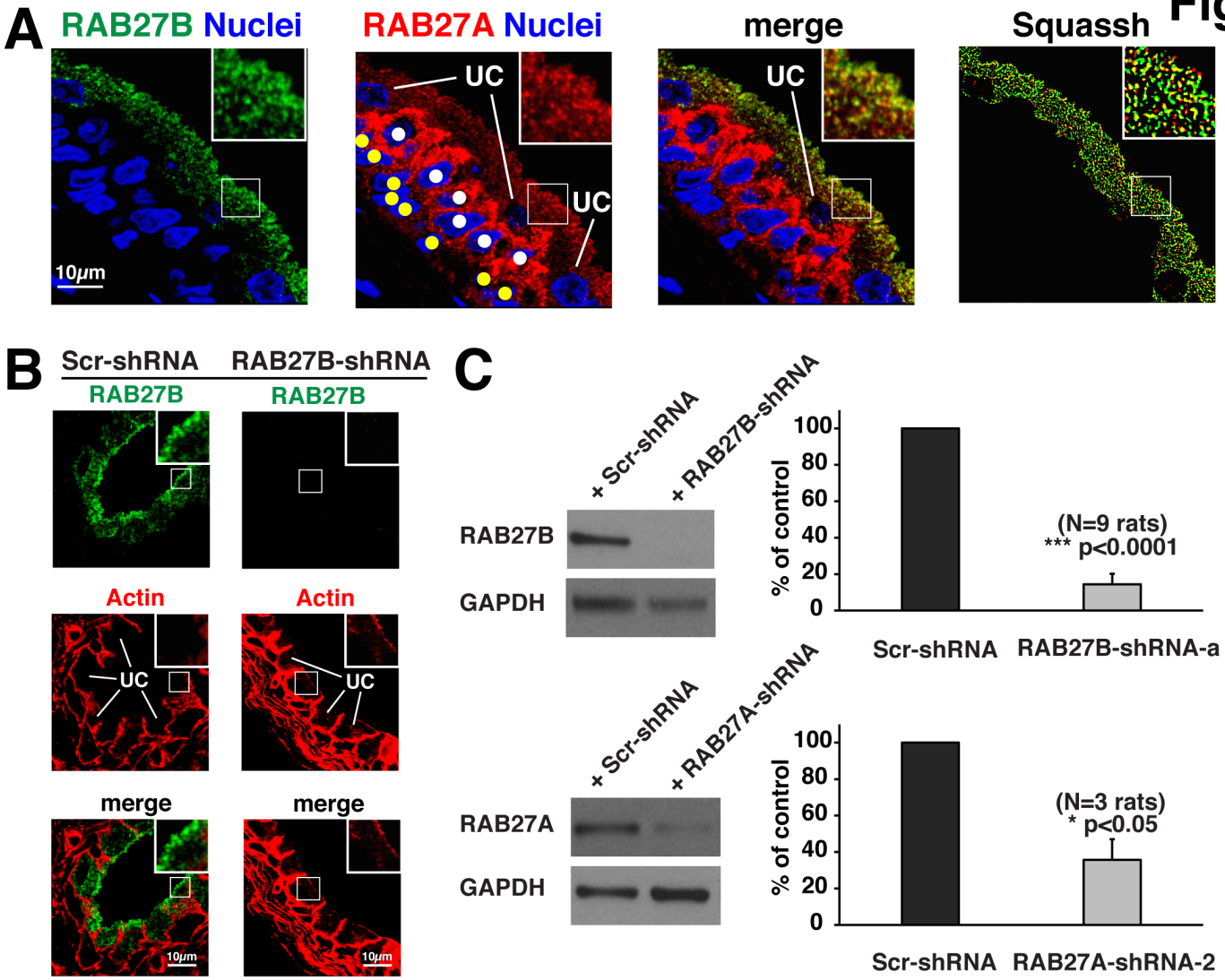

Figure 4

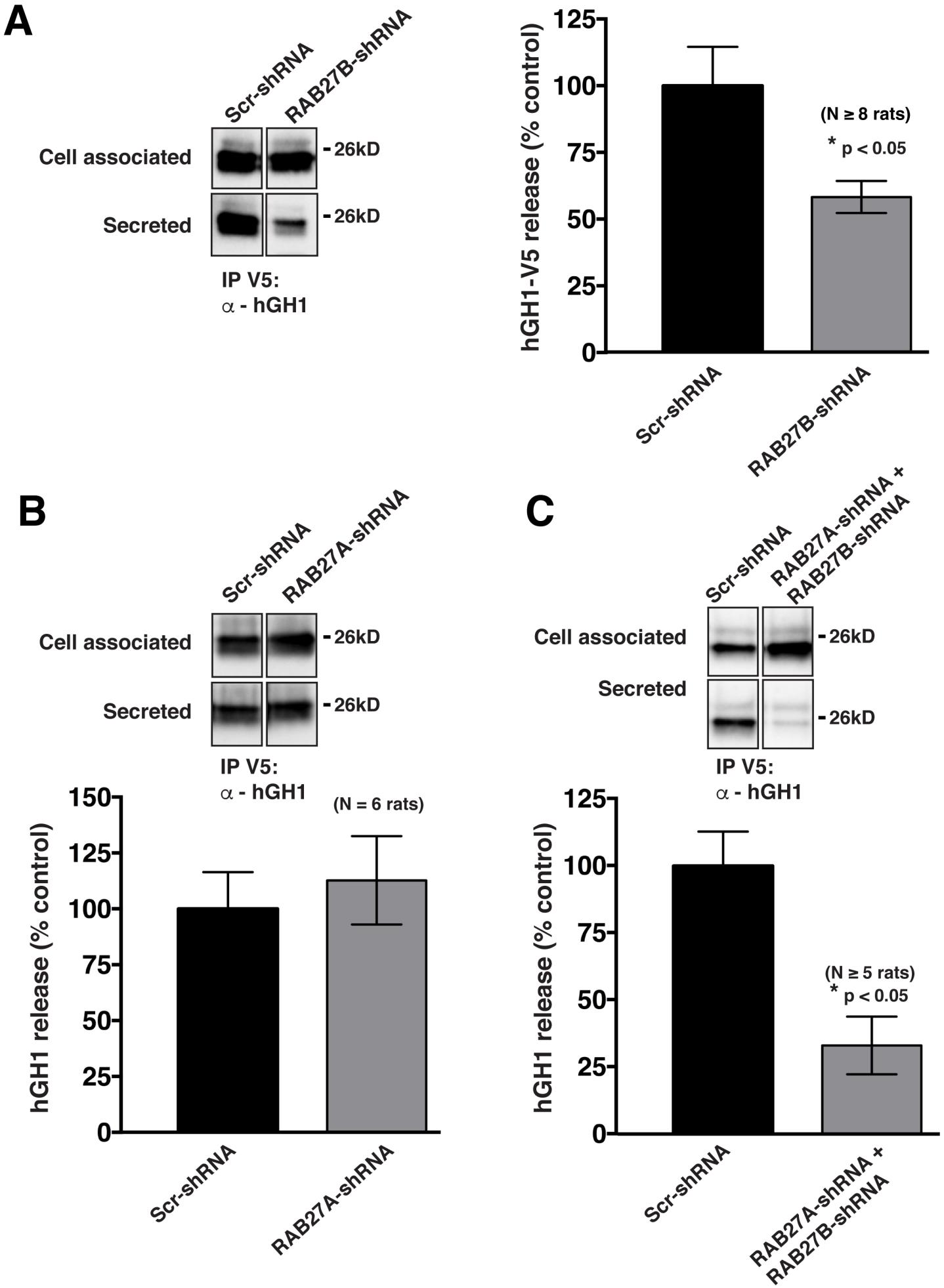

Figure 5

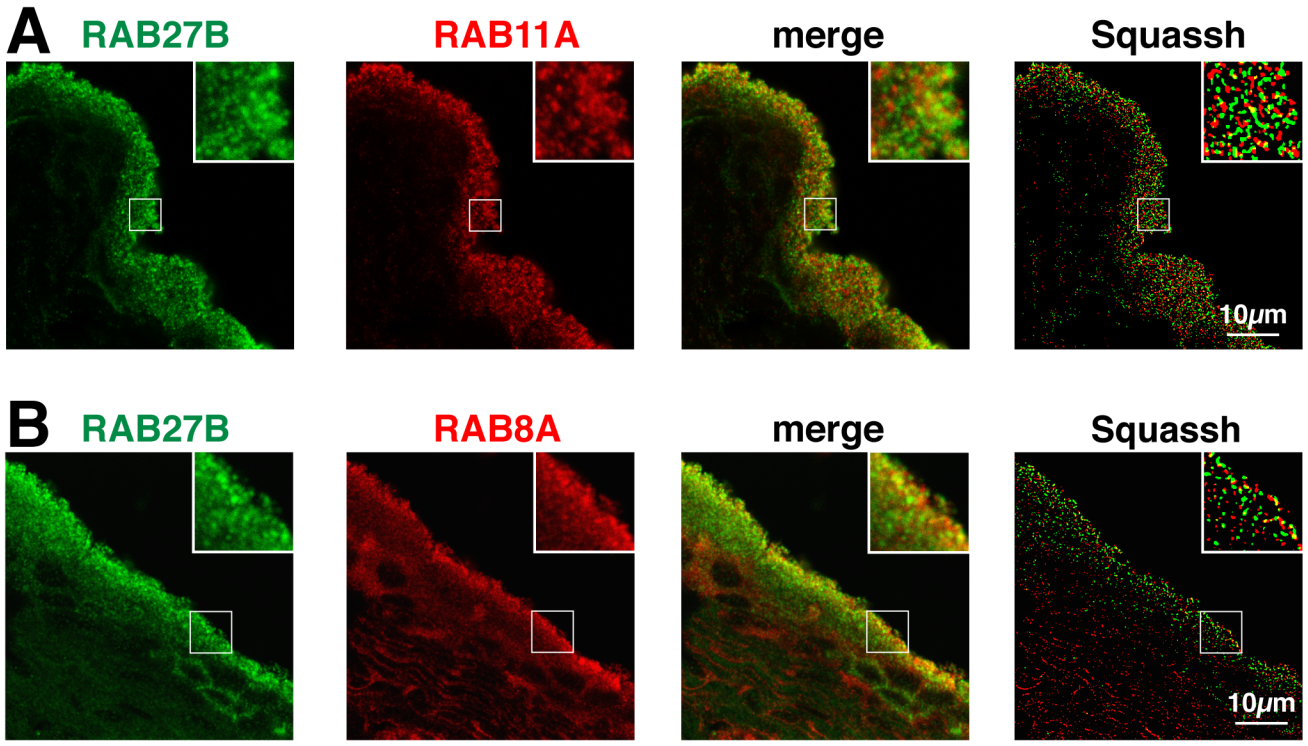

Figure 6

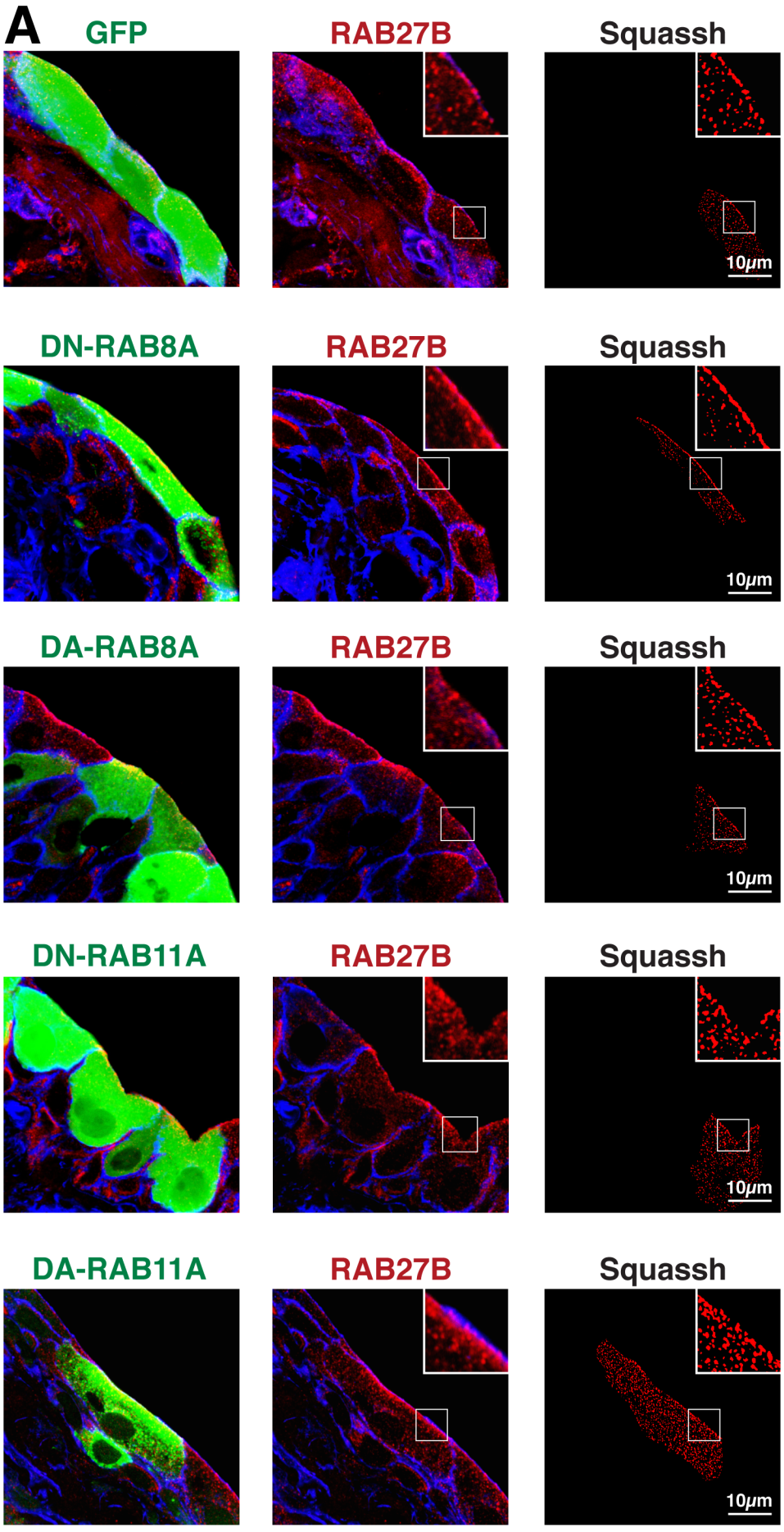

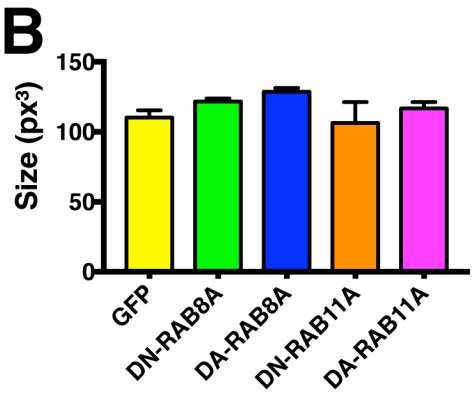

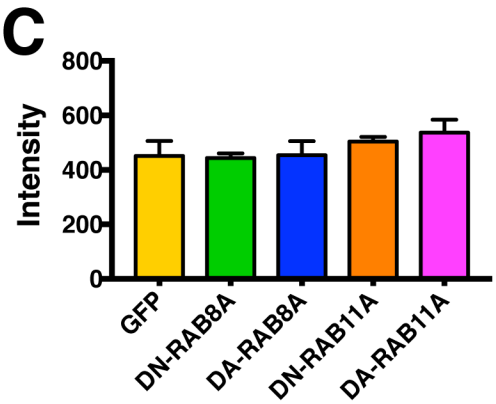

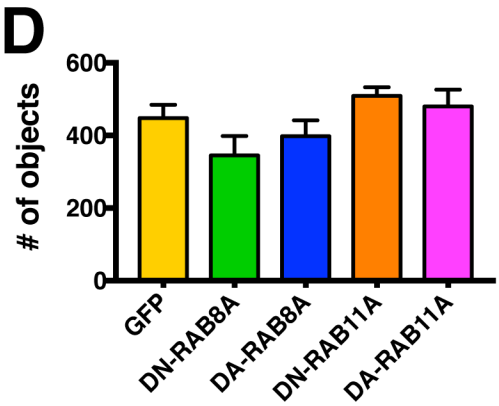

Figure 7

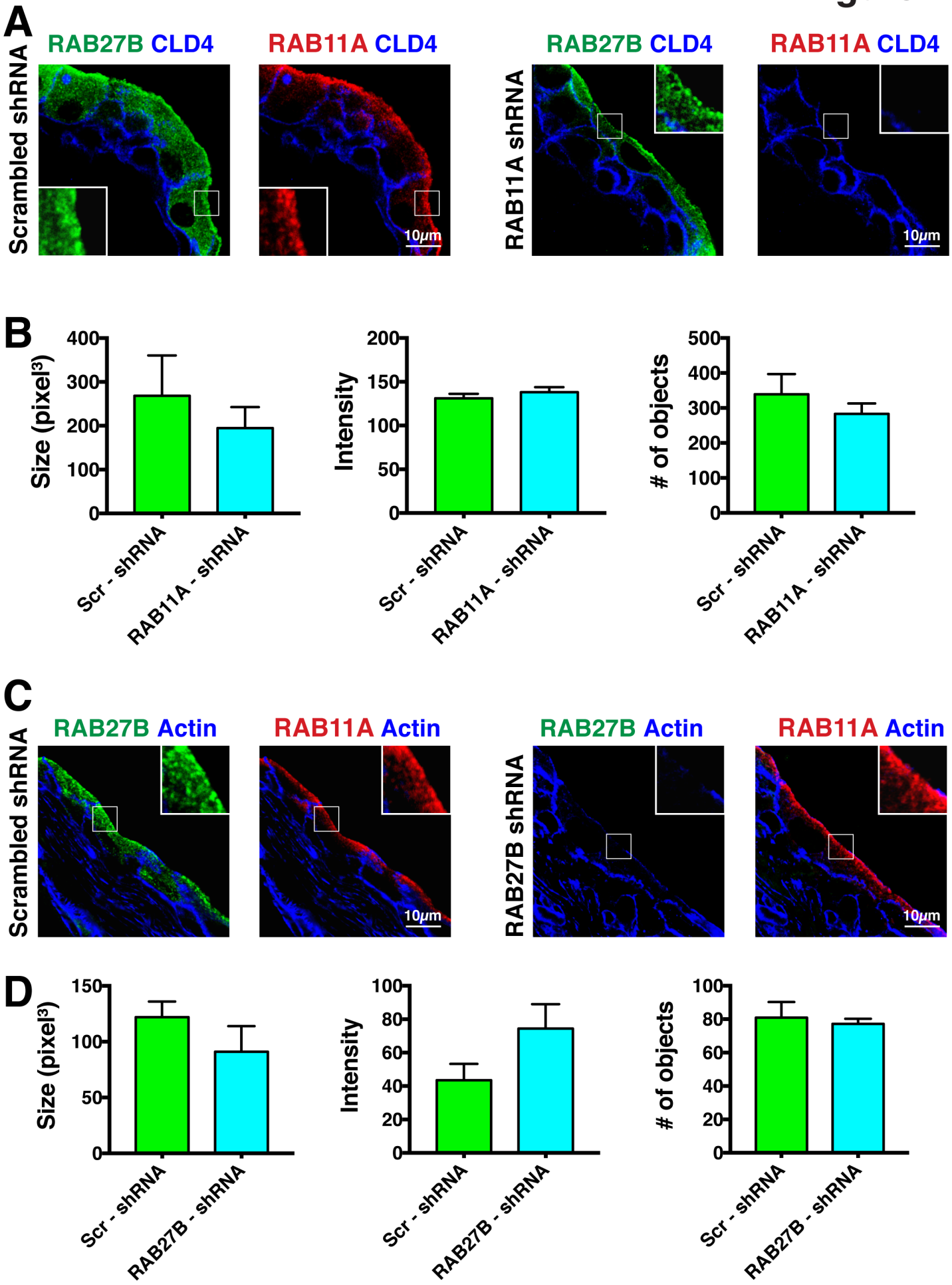

Figure 8

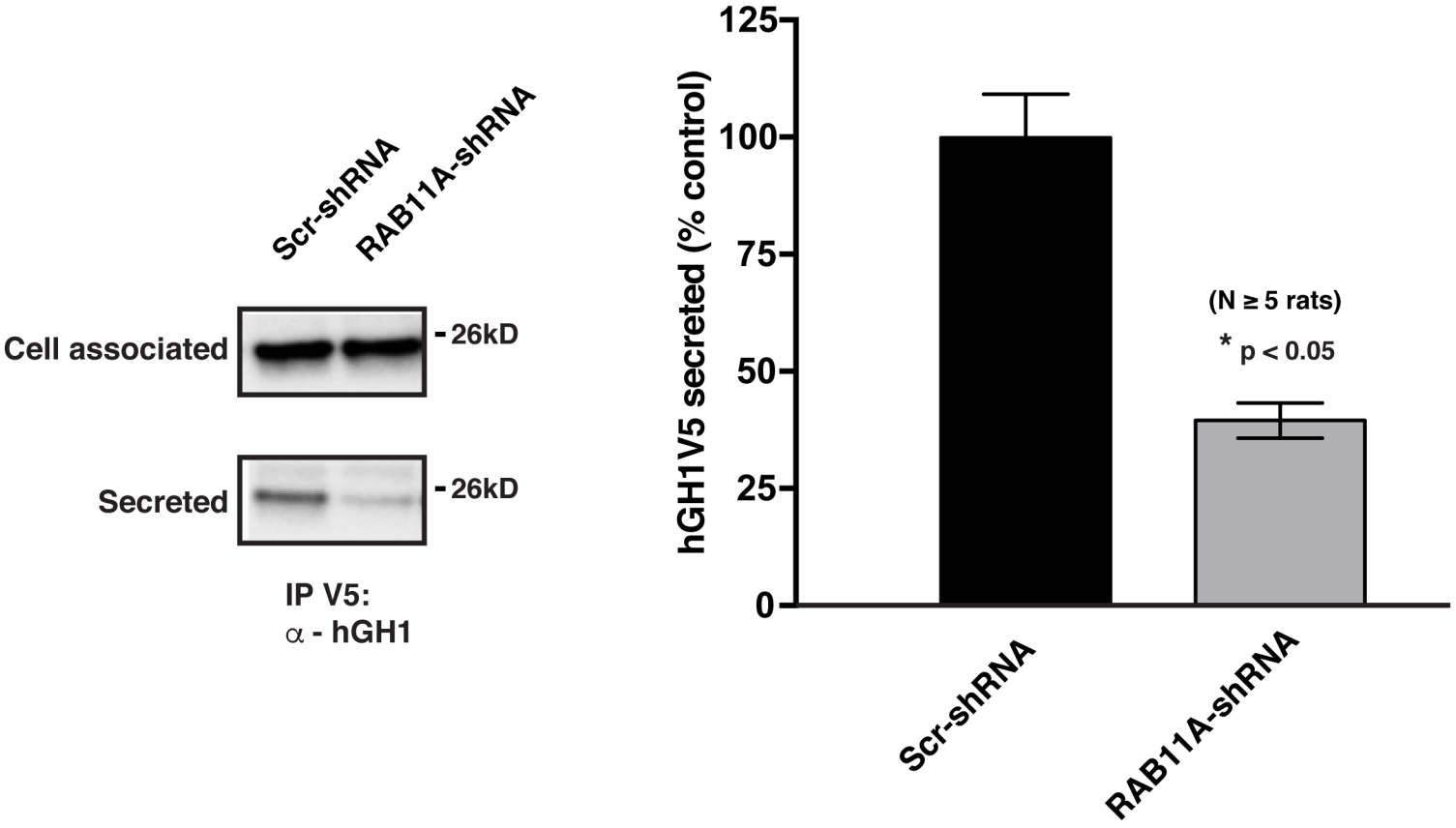

Figure 9